

FEATURE ARTICLE

Surface-Enhanced Raman Scattering: From Noble to Transition Metals and from Rough Surfaces to Ordered Nanostructures

Zhong-Qun Tian,* Bin Ren, and De-Yin Wu

State Key Laboratory for Physical Chemistry of Solid Surfaces and Department of Chemistry, Xiamen University, Xiamen 361005, China

Received: March 10, 2002; In Final Form: July 5, 2002

In the mid-1970s, surface-enhanced Raman scattering (SERS) was discovered which impacted on surface science and spectroscopy because of its extremely high surface sensitivity. However, SERS had not developed as many people had hoped to be a powerful surface diagnostic technique that can be widely used because of some obstacles. For example, only three noble metals Au, Ag, and Cu could provide large enhancement, severely limiting the widespread applications involving other metallic materials of both fundamental and practical importance. In this article, emphasis is put on the recent work of our group to directly generate SERS on net transition metals (e.g., Pt, Ru, Rh, Pd, Fe, Co, Ni, and their alloys) by developing various roughening procedures and optimizing the performance of the confocal Raman microscope. An approach of replacing the randomly roughened surface with ordered nanorod arrays of transition metals is introduced as a promising class of highly SERS-active substrates. The surface enhancement factor for transition metals was calculated, which ranged from 1 to 4 orders of magnitude. The applications of SERS in surface adsorption, electro-catalysis, and corrosion of transition-metal-based systems demonstrated several advantages of in situ surface Raman spectroscopy. A preliminary theoretical approach, considering the electromagnetic and chemical contributions, is presented to explain the SERS behavior of transition metal electrodes and nanorod arrays. It has been shown that SERS together with other surface-enhanced optical phenomena could be one of important issues not only in surface science but also in nanoscale science. Prospects and further developments in this exciting field are discussed with emphasis on the emerging experimental methodology.

1. Introduction

The explosion of activity in the field of surface-enhanced Raman scattering (SERS) started in mid-1970s. The first measurement of a surface Raman spectrum from pyridine adsorbed on an electrochemically roughened silver electrode was reported by Fleischmann, Hendra, and McQuillan in 1974,^{1a} which was stemmed from their pioneering work on applying Raman spectroscopy to the in situ study of electrode surfaces.^{1b–c} The Raman spectrum proved to be of very high quality and evidently was due to a surface species in view of its electrode

potential dependency. In retrospect, this was, in fact, the first SERS measurement although it was not recognized as such at the time. These authors initially thought that the electrochemical roughening procedure has significantly increased the surface area of the electrode so that the intense surface Raman signal of pyridine can be obtained. After carefully making the calculation and experiment, Van Duyne and Jeanmaire realized that the major contribution to the intense Raman signal is due to an enhancement of 10^5 – 10^6 times compared to the intensities predicted from the scattering cross section for the bulk pyridine.² After an exhaustive review process, presumably because of the reluctance of reviewers to believe the unorthodox concept of

* To whom correspondence should be addressed.

surface enhancement, their paper was published in 1977,^{2a} and Albrecht and Creighton independently reported a similar result.³ They provided strong evidences to demonstrate that the enormously strong surface Raman signal must be caused by a true enhancement of the Raman scattering efficiency itself. The effect was later called surface-enhanced Raman scattering (SERS).^{2b}

The discovery of SERS impacted surface science and spectroscopy because of its extremely high surface sensitivity.⁴ As Raman scattering is a second-order process, it has a very low cross section. In the absence of any resonance Raman process, the differential Raman cross sections ($d\sigma/d\Omega$)_{NRS} are less than 10^{-29} cm² sr⁻¹, i.e., generally more than 10 orders of magnitude lower than that of infrared absorption.^{2b,5} Hence, the signal-to-noise ratio (S/N) of the surface Raman signal expected for a monolayer of adsorbates is below the detection limit of a conventional Raman spectrometer. This intrinsically low detection sensitivity is no longer a fatal disadvantage for surface Raman spectroscopy after the discovery of SERS.

The discovery of SERS provided a stimulus for the study of the enhanced optical scattering from metal surfaces. There have been numerous papers dealing with this new physical phenomenon either theoretically or experimentally. Vigorous research activities have ensued not only in the electrochemical environment but also in air and under UHV conditions on virtually every conceivable metal surface morphology: atomically smooth surfaces, thick and thin films coated on smooth and roughened substrates, colloids, powders, and even catalysts supported on insulator granules.⁴⁻¹⁰ A number of experimental characteristics of SERS have been identified. It has been found that SERS differs in a number of ways from ordinary Raman spectroscopy and even from unenhanced surface Raman spectroscopy.⁶⁻¹⁰ More importantly, the effect makes it possible to use SERS as an in situ diagnostic probe for determining the detailed molecular structure and orientation of surface species, which is widely applicable to electrochemical, biological, and other ambient interfaces.^{1c,2b,4,5}

Unfortunately, SERS did not develop to be as powerful a surface technique as many people had hoped because of three obstacles in terms of its practice and theory. First, it turned out in that only Ag, Au, and Cu could provide large enhancement. This severely limited the number of practical applications involving other metallic materials although there are a few reports concerning the SERS from In,^{11a} Ga,^{11b} Na,^{11c} Al,^{11d} Cd,^{11e} Hg,^{11f} Li,^{12a} etc. (vide infra). Second, even for the above SERS active metals, surface morphology with roughness scale of 50~200 nm is crucial to exhibiting a large enhancement factor. These submicroscopic dimensions, fabricated by various surface-roughening procedures, inevitably consist of various microscopic dimensions, such as ad-atoms, ad-clusters, kinks, and vacancies as well as surface complexes. The atomically flat surfaces, commonly used in fundamental research in surface science, are not suitable for SERS investigations. Third, although a number of SERS mechanisms have been proposed to explain the above experimental characteristics for almost three decades, no one mechanism can explain all of the observed effects. There has been the consensus that two mechanisms contribute to the major SERS effect:¹²⁻¹⁵ (i) an electromagnetic (EM) enhancement associated with large local fields caused by surface plasmon resonance and (ii) a chemical enhancement involving a resonance Raman-like process associated with chemical interactions between the molecule and the metal surface. SERS mainly comes about as a combination of the two effects. For the most noble-metal systems, the electromagnetic field enhancement generated from a variety of metal nanostructures

plays a dominant role. Overall, SERS involves complicated interactions and couplings among photon, molecule, and nanoparticles.¹²⁻¹⁵ It seems that the further theoretic work is still required in order to quantitatively explain all SERS phenomena, including simple and complicated ones, which are reported continually.

However, researchers have never given up their efforts to extend SERS to the study of other metallic and nonmetallic surfaces.¹⁶⁻²⁸ In the 1980s, a strategy based on "borrowing SERS" was proposed, either by depositing SERS-active metals onto non-SERS-active substrates, including semiconductors,¹⁶ or by depositing non-SERS-active materials over SERS-active substrates.^{17,18} For example, SERS-active Ag or Au electrodes were coated with ultrathin films of other metals such as Ni, Co and Fe, Pt, Pd, Rh, and Ru by electrochemical deposition. With the aid of the long-range effect of the electromagnetic (EM) enhancement created by the SERS-active substrate underneath, weak SERS spectra of adsorbates on the transition metal overlayer can be obtained.^{17,18} It should be noted that the strong electromagnetic field generated on the SERS-active substrate is damped significantly by the coated film so that the film has to be ultrathin, normally 3-10 atomic layers. It was very difficult to cover completely rough substrates with such a thin film. Thus, the "pinhole" in the overlayer made it extremely difficult to eliminate entirely the contribution of the giant SERS of the substrate. Recently, Weaver and co-workers have made a significant progress to overcome this problem. They reported a series of work on "pinhole-free" transition metal over the SERS-active Au surface by electrochemical atomic-layer epitaxy using constant-current deposition at a low current density or by redox replacement of underpotential-deposited metals on Au.¹⁹ It has been shown that this method is very promising if one can prepare the "pinhole-free" ultrathin film for different materials with good stability in a wide range of potential or/and temperature. It makes SERS a versatile tool in studying various material surfaces of practical importance. In addition to studying surface adsorption and reaction, the overlayer method can be used to characterize the fine structure of ultrathin film itself. This includes oxides, semiconductors, and polymers.²⁰ Its advantage of high sensitivity enables one to probe ultrathin film with a few atomic monolayers. Without the aid of SERS, Raman spectroscopy is rather possible using rather thick films with thickness ranging from submicron to micrometers.^{1b,c,21}

Another totally different strategy is to generate SERS directly from transition metals. There is no doubt that the surface preparation is more straightforward and the stability is higher than the substrate coated with the ultrathin film. This strategy is much more challenging as it contradicts to the commonly accepted notion that transition metals were not SERS active. This approach appeared the most difficult or even impossible one and has been demonstrated since the early days of SERS. Several groups attempted to obtain unenhanced²²⁻²⁴ and enhanced^{25,26} Raman signals from adsorbates on either roughened or mechanically polished Pt and Rh electrodes, or porous Ni, Pd, Pt, Ti, and Co films.²⁷ In all of these research efforts, the reported surface spectra were obtained only under optimal conditions or by data manipulation using spectral subtraction methods.²²⁻²⁴ Surface Raman signals were typically too weak to be investigated as a function of the electrode potential or temperature although this is essential for practical applications. The worse thing was that some results could not be able to be repeated by other groups. The reported results were not strongly supportive of SERS studies on transition metals and point to a

gloomy future in this direction. Indeed, only a few papers,^{26,28} among many theoretical and experimental works, claimed that transition metals might have relatively weak SERS activity in comparison with the noble metals of Au, Ag, and Cu but had not been recognized by the scientific community. As a consequence of the abovementioned obstacles, the activity in the SERS field declined substantially from the late-1980s to the late-1990s. To our knowledge, there had been no reports on observation of SERS directly from net transition metals in the past 10 years except our group and Li and Yang and their co-workers who reported SERS from iron nanoparticles very recently.^{26d}

In our opinion, the development of SERS is both fascinating and frustrating as its advantages and disadvantages are both so significant. It should be noted that SERS is not a unique phenomenon but belongs to the family of surface-enhanced optical spectroscopy. After discovering SERS, people also found surface-enhanced second harmonic generation,²⁹ infrared absorption,^{30,31} fluorescence,³² and sum frequency generation.³³ Therefore, there may be some fundamental scientific basis underlying the complex phenomena of surface-enhanced optical spectroscopy. It is truly a great challenge but a difficult task to elucidate SERS by comprehensively examining the process, its origin, experimental details, etc. Hence, many groups including ours have been working hard along this avenue for years in seeking ways to overcome the three obstacles mentioned before.

The situation has changed dramatically since the late-1990s,³⁴ with advances in Raman instrumentation and the advent of the confocal microscope and the holographic notch filter.³⁵ The Raman experiment, which normally employed high-dispersion double or triple monochromators to filter out the elastically scattered laser radiation, can now be performed simply with a single spectrograph together with a holographic notch filter. The throughput of a single-grating system is far higher than, for example, a triple monochromator. The optical configuration of the confocal Raman microscope was found to be very helpful for obtaining the very weak signal of the surface species without the interference of the strong signal from the bulk phase. These new developments have resulted in unprecedented sensitivity that is vitally important for making some important advances in this field in the late-1990s.

One of the progresses is the confirmation of SERS directly from many net transition metals.^{36,37} Since 1996, our group has made efforts to optimize the confocal Raman microscope in order to obtain the highest sensitivity and to develop special surface roughening procedures to obtain large enhancement factors. Several pretreatment procedures for different transition metals have been examined so that good-quality surface Raman signals have been obtained from bare Pt, Ru, Rh, Pd, Fe, Co, and Ni electrodes.³⁷ It has been found that transition metals exhibit surface enhancement factors ranging from 1 to 4 orders of magnitude, depending on the nature of metal and the surface morphology.^{36,37c-e} The results demonstrate the importance of establishing appropriate surface pretreatment procedures for obtaining SERS effect from the transition metals.^{36,37} The molecular-level investigation by Raman spectroscopy on diverse adsorbates at various transition metals has been realized.

The most significant progress is to bring SERS into the forefront with single-molecule Raman spectroscopy, largely through the pioneering work by Kneipp³⁸ and Nie^{34a,39} and their co-workers. The high-quality SERS or surface-enhanced resonance Raman scattering (SERRS) spectra from a single molecule adsorbed on the surface of silver and gold particles or the aggregated colloids can be obtained. The estimated signal

enhancement surprisingly amounts up to $10^{14}\sim 10^{15}$, which is much higher than the widely accepted value of 10^9 . This has re-energized the research field substantially.³⁸⁻⁴⁰ As this topic is beyond the scope of this article, for the readers who are interested, some excellent review articles and interesting papers are highly recommended.^{12c,13c,34a,b,d,38-40}

Actually, people have already realized that most SERS-active surfaces are nonuniform since a long time ago.^{41,42} On a SERS-active substrate, some spots or sites exhibit much higher SERS activity than other areas. Moskovits and Shalaevev and their co-workers have investigated this phenomenon especially from the theoretical point of view and named the highly active spots as "hot spots".⁴² The recent progress in SERS from single nanoparticles and specific nanoparticle aggregates, with the help of TEM and AFM characterization, has provided a much clearer picture than before. It is of particular interest that nanoparticles of different sizes and shapes could have very different enhancement effect. For example, the particles (or aggregates) with size of about 90 nm have the highest enhancement for Ag,^{39b} whereas it is around 60 nm for Au.^{39c} It is evident that the 10^{10} times enhanced single molecule signal was due to a molecule existing in the interstices or sharp clefts of two Ag nanoparticles separated with a distance of about 1 nm.^{40a} These approaches provide a great opportunity to obtain a deeper insight into the nature of hot nanoparticles, hot spots, and active sites.^{12,13,38-42} It also suggests that the SERS substrates with ordered and appropriate surface nanostructure may have much higher activity. Accordingly, it is of special interest to extend the SERS substrate from randomly rough surfaces to ordered nanostructures.

Several approaches to preparing ordered periodic arrays of nanoparticles for SERS have been made since the 1980s. The first one was reported by Liao et al. in the early 1980s.⁴³ They obtained regularly ordered SERS substrates by depositing Ag particles over periodic arrays of silica posts that were fabricated by photolithography. Because of the limitation of the spatial resolution of the lithography at that time, the particle size was as large as about several hundred nanometers that is not an optimal size. Since the mid-1990s many nanofabrication techniques have been developing rapidly. It provides a good way to fabricate a variety of nanostructures for use as new SERS active substrates. One of the most significant approaches has been proposed and developed by Natan and co-workers based upon the self-assembled monolayer technique.⁴⁴ It allows one to prepare regularly arranged monodispersed colloidal gold and silver particles on functionalized metal or glass substrates, producing SERS with good reproducibility and stability.^{44,45} Another important ability of this method is to control the particle size and density, and the space between the substrate and the particle, thus to tune the electromagnetic characteristics of the surface for systematic study of the SERS mechanism.

Recently, Van Duyne and co-workers have made special effort to broaden the scope of nanosphere lithography to fabricate several new nanoparticle structural motifs.⁴⁶ The silver metal is evaporated on preformed arrays of nanopores which are then removed, leaving behind the metal particles formed in the interstices. These methods have been demonstrated to be well suited for the synthesis of size-tunable noble-metal nanoparticles in the 20–1000 nm range. They have used localized surface-plasmon resonance spectroscopy very successfully to probe the optical properties of size tunable Ag nanoparticles and to systematically investigate the effects by nanoparticle size, shape, interparticle spacing, nanoparticle–substrate interaction, solvent, dielectric overlayers, and molec-

ular adsorbates.⁴⁶ Most recently, Park et al. used transition-metal salts (H_2PtCl_4 and PdCl_2) to oxidize and replace previously underpotential-deposited Cu layer over Au colloids that have been immobilized on an ITO surface.⁴⁷ This new approach of using the overlayer technique can generate SERS from a transition-metal coated surface that is capable of potential control. These methods will be very useful in further investigating the complex behavior and mechanism of SERS, which is one of the most fascinating fields of size-dependent nanoparticle optics.

It should be pointed out that SERS activity depends on both the size and shape of the particles. Many theoretical work based on the electromagnetic enhancement have predicted that SERS intensity will increase significantly with the increase in the aspect ratio of the nanoparticles.^{4,12,14,28} It has been well-known that nanorod (or nanowire) arrays can be fabricated by means of template synthesis.⁴⁸ The advantage of this method is its flexibility to precisely control the diameter and especially the aspect ratio of nanorod arrays. Thus, ordered nanorod arrays could serve as a new class of SERS-active substrates especially for transition metals. Through previous works and our study, it has been shown convincingly that SERS is one of the important phenomena not only in surface science but also in nanoscale science (vide infra). As a whole, the exciting progresses mentioned before have led us to believe that a revival of interest in SERS study is forthcoming.

In this article, emphasis is put on recent work of our group, i.e., the generation of SERS on transition-metal substrates using various roughening procedures, the optimization of the performance of the confocal Raman microscope, calculation of the surface enhancement factor, and the application of SERS to problems in electro-catalysis and the corrosion of transition metals. We will demonstrate that it is now possible to carry out detailed molecular-level investigations by SERS on diverse molecules at many substrates that were not commonly considered as SERS active systems, at least in practice. Then, we will introduce a new approach of replacing the randomly roughened surface with ordered nanorod arrays of transition metals having a narrow size distribution for use as good SERS-active substrates. To explain the SERS behavior of transition-metal electrodes and nanorod arrays, a preliminary theoretical approach, based on the standard electromagnetic and chemical enhancement mechanisms, is presented and compared with that of "free-electron" metals. Finally, some recent developments and possible future directions with emphasis on the emerging experimental methodology are discussed.

2. Experimental Section

2.1. Strategies to Increase Detection Sensitivity. In studying transition-metal surfaces, it is essential to increase the detection sensitivity in every aspect. We will focus here on how to increase the detection sensitivity of the Raman instrument. On the basis of the quantum mechanical theory of light scattering, Placzek's polarizability theory, the normal surface Raman intensity arising from a transition between the vibrational states m (ν_m) and n (ν_n) is given by⁴⁹

$$I_{mn} = \frac{2^7 \pi^5}{3^2 c^4} I_0 (\nu_0 - \nu_m)^4 \sum_{\rho\sigma} |(\alpha_\rho \sigma)_{mn}|^2 N A \Omega Q T_0 T_m \quad (1)$$

where I_0 is the power density, ν_0 is the frequency of the exciting light, $\nu_{mn} = \nu_n - \nu_m$, $(\alpha)_{mn}$ is the component of the polarizability tensor, N is the number density of the adsorbate (molecules cm^{-2}), A is the surface area illuminated by the laser beam (cm^2), Ω is the solid angle of the collection optics (steradian, sr), and

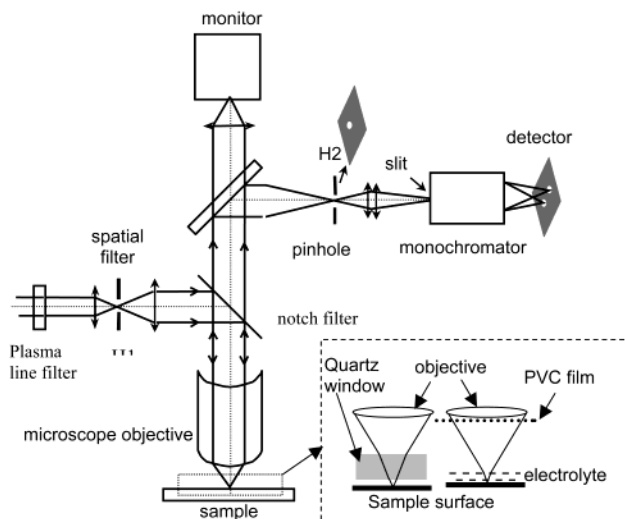


Figure 1. Schematic diagram of a confocal microprobe Raman system. Insertion: the two possible configuration of the experimental setup between the collection microscope objective and the electrode surface.

QT_0T_m are the product of the detector efficiency, the transmittance of the collection optics, and the throughput of the dispersion system.

Accordingly, to increase the detection sensitivity of the Raman instrument, several factors have been carefully considered to improve ΩQT_0T_m : (1) using a microscopic setup with a microscope objective of wide numerical aperture to increase the solid angle (Ω) of the collection system, (2) utilizing the confocal configuration to eliminate stray light, (3) employing a CCD detector of very low dark current and high quantum efficiency (Q), and (4) using a holographic notch filter to reduce the number of optical components and so as to increase the throughput (T_0T_m) of the spectrometer.

2.2. Confocal Raman Microscope. The Raman instruments employed in the present study belong to a new generation of Raman spectrometers, i.e., LabRam I and Renishaw UV1000 confocal microprobe Raman systems. A schematic diagram of the LabRam I system is shown in Figure 1. The system utilizes a backscattering configuration to collect the Raman signal through a microscope vertically. The microscope uses a $50\times$ long working-length objective (the working length is 8 mm, the NA is 0.55) so that the objective would not be immersed in the electrolyte for in situ measurements. A holographic notch filter is used to filter the excitation line from the collected light. A thermoelectrically cooled CCD 1024×256 pixels operating at about -60°C is used as the detector. Equipped with an X-Y stage, the instrument is capable of performing surface Raman imaging. Exciting wavelengths of 632.8 nm from an air-cooled He-Ne laser and 514.5 nm from an Ar^+ laser are employed. The laser power could be adjusted and the laser spot size is ca. $1\sim 2\ \mu\text{m}$.

Because the collection efficiency of the system is greatly dependent on the optical alignment, proper design of the spectroelectrochemical cell is crucially important. On one hand, it should have a minimum loss of the signal. On the other hand, it should not impede the electrochemical process. In some cases, the cell should also allow for exchanging the solution or purging with gas during the experiment.

In the confocal configuration, the laser is focused on the sample surface with a microscope objective. A pinhole with controllable size (H_2 in Figure 1) is installed at the right position of the image of the illuminated sample point. Hence, only signals from the volume very close to the focal point can be focused

and pass through the pinhole (as the confocused spot) to be imaged by the detector. The signal from the off-focus region cannot be imaged by the detector, thus minimizing the influence of the bulk signal on the surface layer to be analyzed. This configuration has been shown to be very helpful for obtaining the very weak signal of surface species without the severe interference of the bulk signal, e.g., that of the solution species. The size of the slit and confocal pinhole could be adjusted to meet the requirement of the individual experiment.

2.3. Optimization of the Experimental Setup. The signal collection efficiency is significantly influenced by the transmittance and throughput of the Raman system (T_0T_m). The microscope objective plays a key role in microscopic systems as it introduces the laser and collects the Raman signal. To maintain aberration corrections of the objective for a good alignment and for high T_0T_m , the refractive index (n) of the media must be closely matched. However, it should be emphasized that the commercial Raman systems are not built for a special applications, such as for detecting extremely weak signals from the electrode/electrolyte interface. The Raman system is normally designed with the presumption that the medium between the objective and the sample surface is air. In an electrochemical system, the matching requirement cannot be strictly met, because there are several media of various indices n between the electrode surface and the objective, e.g., air, the cover-glass (or quartz window), the solution phase, etc.; this results in serious performance degradation. It prevents the Raman signal of the surface species from passing through the pinhole to the detector. Without making a careful optical alignment of the electrochemical cell, the advantage of the confocal microscope is lost, and the surface Raman signal may not be detected. For example, a solution layer of large n could affect dramatically the collection efficiency of the microscope by decreasing the solid angle (Ω) of the system. With an increase in the thickness of the solution layer from about 0.2, 0.5, or 1 mm to 2 mm, the Raman signal intensity decreases from 89%, 71%, 52%, and 35%, respectively, of the maximum intensity in air. A thickness of 0.2 mm appears to be optimum for electrochemical system.

Furthermore, in the electrochemical system, most of the electrolytes are corrosive, so that in order to protect the objective, a cover glass or quartz window has to be employed between the electrolyte and the objective; this results in a 50% loss of the signal. An alternative and the best way, we found, to protect the objective is to wrap it with a very thin and highly transparent poly(vinyl chloride) (PVC) film. With this approach, the Raman signal only suffers a 10% loss. Hence, optimization of the optical configuration is essentially important in order to realize the full potential of confocal Raman microscopy.

The CCD detector has different quantum efficiency for different wavelengths, so an optimization of its wavelength response can increase the sensitivity by a factor of 2–4. To realize the potential of the CCD detector, the pixels in the CCD element can be binned within the chip (although at the expense of spectral resolution) to increase the signal-to-noise ratio (SNR). It can be used to detect extremely weak Raman bands that extend over a large number of pixels. In our present study, because of the very weak Raman signal, this binning strategy has to be employed to increase the SNR. The spectral resolution after binning 2 pixels still meets the requirement of separating the vibrational bands of the surface species. Overall, the optimization of the microscope objective, the confocal setup, and the use of the CCD detector can improve the sensitivity of the Raman system by a factor of more than 1 order of

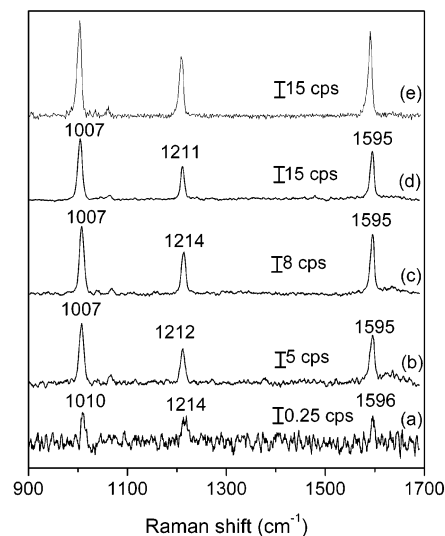


Figure 2. Raman spectra of pyridine adsorbed on nickel surfaces roughened by using different procedures (a) mechanically polishing, (b) chemically etching in 1 M HNO_3 , (c) ex situ oxidation and reduction in 0.1 M KCl by stepping the potential from -0.4 to $+0.4$ V where the potential was held for 3 s and then returned to -0.4 V, (d) in situ ORC in 0.01 M pyridine + 0.1 M KCl in the spectroelectrochemical cell prior to the measurement, and (e) nickel nanowires prepared by template methods. The exciting wavelength: 632.8 nm. Solution: 0.01 M pyridine and 0.1 M KCl.

magnitude. This value is absolutely necessary for obtaining the weak signal from transition-metal systems.

3. Results and Discussion

3.1. Surface Roughening Procedure for Transition Metals.

As has been well-known from previous SERS studies on Au, Ag, and Cu, a necessary, but not sufficient, requirement for large surface enhancement is some form of surface roughness.^{1–5} The surface pretreatment is even more important for getting the surface Raman signal from transition metals that were considered as non-SERS active. Because SERS appears to be an all-or-nothing effect in the measurement, one must make great effort to optimize the SERS activity of the transition metal. It is reasonable to put this story as the first part of this section, instead of in the Experimental Section, for a detailed description and discussion. In the past five years, we have examined and developed various surface-roughening procedures for different transition metals to obtain surface spectra with better SNR.

Figure 2 is a typical example illustrating the distinct effect of the surface roughening procedure on the Raman intensity of pyridine adsorbed on Ni electrode surfaces.^{37c} The surface signal is extremely weak from the mirrorlike surface prepared by mechanical polishing with alumina powders down to 0.05 μm . The strongest band intensity for the adsorbed pyridine is only about 0.5 cps (Figure 2a). Clearly, the spectrum recorded is too weak to allow further investigation as a function of potential. The signal-to-noise ratio (S/N) was improved considerably after the electrode was chemically etched in a 1.0 M solution of HNO_3 (10 cps in the strongest band). The signal intensity increased to about 24 cps if the electrode was further treated in a 0.1 M KCl solution using a double-potential step oxidation–reduction cycle (ORC). An even more intense signal of 50 cps was obtained when an additional ORC was performed in situ in the spectroelectrochemical cell prior to the measurement. The highest intensity (80 cps) can be obtained from a Ni nanowire array. This set of spectra show that a proper surface roughening procedure is key to obtaining good spectra from transition metals.

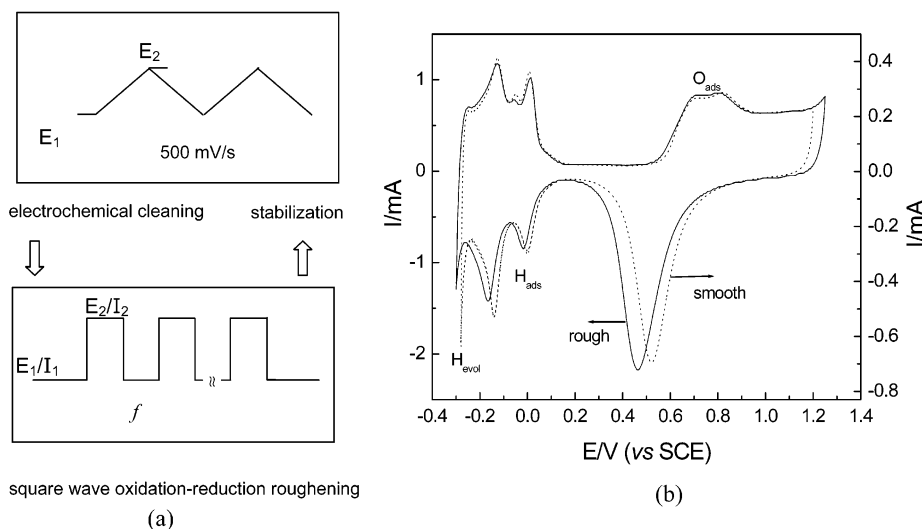


Figure 3. (a) Illustration of the roughening procedure for Pt and Rh surface by using square-wave potential (by controlling the E_1/E_2) or current (by controlling the I_1/I_2) oxidation–reduction method. The solution used is 0.5 M H_2SO_4 . (b) A comparison of the cyclic voltammograms of roughened (—) and smooth (···) Pt electrodes in 0.5 M H_2SO_4 solution. Scan rate: 50 mV/s.

3.1.1. Electrochemical Oxidation–Reduction Cycle (ORC).

This roughening procedure is the most important method, at least in the present stage, so it will be discussed in more detail. Experimental variables in the ORC include the oxidation and reduction potentials, the type of potential–time function (e.g., triangular-wave potential sweep or double potential steps), the amount of charge passed for each oxidation step or sweep, the number of cycles, and the composition of electrolyte.^{4,5}

Because transition metals are distinctively different from “free-electron” metals in terms of electronic structure, and chemical properties, it is important to develop different kinds of ORC procedures to optimize the SERS activity. Some very stable metals, such as Pt and Rh, are very difficult to roughen by the dissolution and deposition of the surface atoms. These metals tend to form a compact oxide layer that prevents further oxidation of the surface; thus, it is nearly impossible to form an optimal size for SERS activity. To establish an appropriate surface roughening procedure and obtain high-quality surface Raman spectra from Pt electrodes, various conditions have been examined. For electrochemical studies, Arvia and co-workers established a unique roughening procedure for Pt electrodes. A Pt electrode of large surface area can be obtained in acidic electrolytes via the electroreduction of a previously formed thick hydrous Pt oxide layer by applying a repetitive periodic potential.⁵⁰ In the present study, some modifications of the surface roughening procedure have been made to get a stronger surface Raman signal. It can be realized by applying a high-frequency alternating voltage with high oxidation potential and mild reduction potential.

As shown in Figure 3, the Pt electrode is subjected to a square wave potential ($E_1 = -0.20$ V, $E_2 = +2.4$ V, $f = 0.5\sim 2$ kHz) oxidation and reduction cycles (ORCs) in a fresh sulfuric acid solution for a few seconds to several minutes depending on the purpose of the study.^{36a–c,37a} The high-frequency voltage applied enables the exchange of the surface oxygen with the bulk metal atoms leading to the further oxidation of the inner layers of the surface. After that, the electrode potential is kept at -0.20 V for complete reduction. The surface roughness factor (R) for the Pt ranged from 30 to 500 which can be obtained by varying the roughening time and the applied potential and the frequency.^{36c} The color of the electrode varies from light yellow to gray, depending on the parameters used for the ORC and the stabilization time. The STM image of the highly rough Pt surface

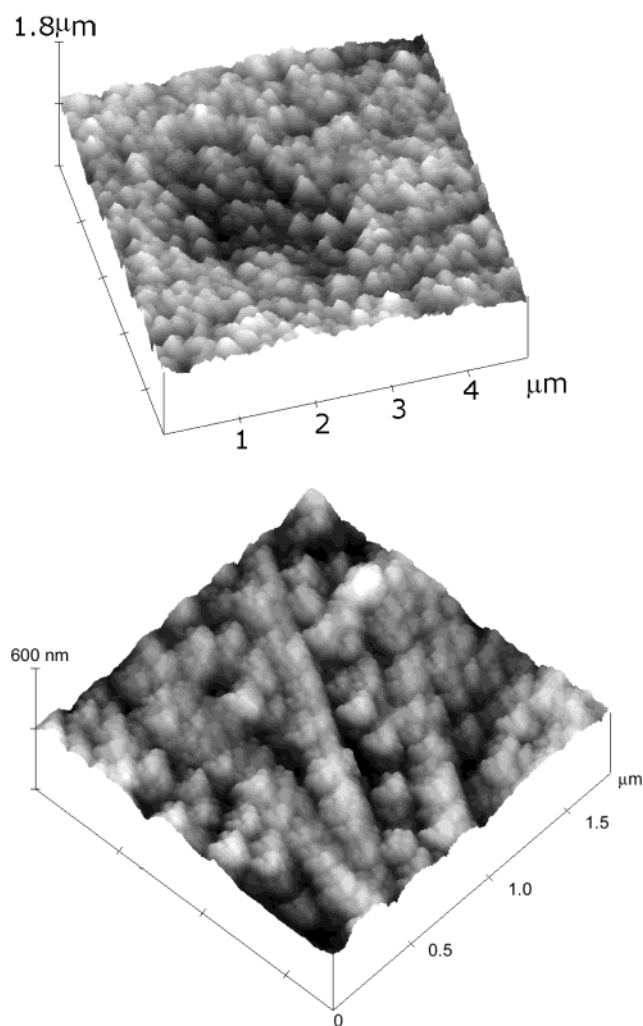


Figure 4. (a) The STM image of a Pt electrode after electrochemical roughening treatment by controlling the oxidation and reduction potential. (b) The AFM image of an Rh electrode after electrochemical roughening by controlling the oxidation and reduction current.

(with $R \approx 200$) is given in Figure 4a. It can be seen that the Pt surface presents a very rough but quite uniform structure, and bumps about 200 nm high are present. Zooming on a smaller

area, some fine structures (around 10–20 nm) on the 200 nm bumps can be seen. This is evidence for the large enlargement of the surface area.

3.1.2. Current Controlled ORC. The Rh electrode is more difficult to roughen by applying a square-wave potential, which is very effective for obtaining a Pt electrode of high surface area and moderate SERS activity. After a systematic study, we found that the rhodium surface can be effectively roughened in 0.5 M H₂SO₄ by applying a square-wave current of +40 and –30 mA with the frequency between 200–800 Hz.⁵¹ The electrode potential was thereafter held at –0.2 V until the completion of the surface electroreduction. Details of the electrochemical roughening procedure are similar to Pt, except that a square-wave current was applied instead of square-wave potential. It should be emphasized that in the case of the controlled current, the electrode surface reaction rate is well controlled, so that the oxidation and reduction rates are defined. This newly developing method is in contrast to the conventional potential controlled mode by which the oxidation and reduction rates are changing with the time. The AFM image Rh surface after such kind of roughening is shown in Figure 4b, in which it also presents some nanoparticles in the range of 10–20 nm on the 100 nm particles. The controlled current method has an advantage in well controlling the surface roughening rate, which is important for obtaining more uniform surface morphology. It is also very effective for other metals, e.g., a Pt electrode of low surface area but high SERS activity. However, the current and frequency are very different from those for Rh, depending on the metal.

3.1.3. Chemical Etching. This is a relatively simple tactic for roughening metal surfaces which partially dissolves surface atoms via chemical reaction.⁵² However, it also requires experimental skill to optimize the SERS activity for different metal samples.⁵² For example, Ni electrodes were immersed into 1 M HNO₃ solution and etched for about 5–7 min. A sponge-type surface with substantial roughness resulted.^{37c} For Fe surfaces, the best result was obtained by etching in an ultrasonic bath with 2 M H₂SO₄ for 5 min until the surface turned gray.^{37d}

For some metals, chemical etching is not sufficient to obtain the optimal surface roughness for SERS shown in Figure 2. One may then consider a further SERS activation of the chemically etched electrode by ORC either in the chemical etching solution (*ex situ*) or in the electrolyte solution (*in situ*). The roughening procedure for Fe and Co is similar but not identical to that for Ni. Slight differences in etching time, solution, and *ex situ* pretreatments are required.

3.1.4. Film Deposition. In contrast to chemical etching, this method deposits some atoms on the substrate to form a rough film and/or discontinuous islands. This can be done by vacuum or sputter deposition of the metal on some suitable substrates, including silica slides, graphite, or glass. A rough film can also be prepared by electrochemical deposition of the metals onto smooth electrode surfaces in solution containing the metal ions. It should be noted that this method is much easier and more flexible than that of the aforementioned “overlayer technique”, in terms of film thickness and uniformity. The film can be deposited with various thicknesses ranging from a few nanometers to several hundred micrometers. However, the overlayer method can provide a stronger SERS signal with the aid of high SERS-active metal underneath the overlayer. By controlling the deposition rate and time, reasonably good-quality surface Raman signals from thick transition-metal films, such as Ru, Rh, Pd, Ni, Co, and Fe, have been obtained.^{37b} However, the film electrode is unlikely to have the same crystalline structure as

the bulk phase. Thus, this method is not used often unless we are unable to obtain the massive metal.

3.1.5. Template Synthesis of Metal Nanowire Arrays. The randomly rough surfaces described above have a rather broad distribution of roughness, i.e., from angstroms to micron as can be seen in Figure 4. This ill-defined geometry is most unfavorable for theoretical modeling of the SERS mechanisms. It has indeed led to some debatable issues, e.g., which portion (or scale) of surface roughness plays a major role in the SERS activity. More importantly, the highest activity may require a very narrow distribution of roughness feature of certain size and shape. Thus, a well-controlled nanostructured surface is highly desirable. In 1995, Joo and Suh reported that Ag nanowires were electrochemically deposited into the nanopores of anodic aluminum oxide (AAO) films followed by partial removal of the oxide layer to give rise to a SERS signal.^{48d,e} The result obtained did not attract much attention as the SERS intensity they obtained was weaker than that from normally prepared Ag colloids. So the authors did not continue their work along this avenue. We thought that the noble and transition metal nanowire arrays may exhibit strong SERS activity, especially with careful preparation of suitable diameter and length.^{48f,g}

Figure 5A shows a schematic diagram of the fabrication procedures for our metal nanowire arrays. First, the aluminum substrate was electrochemically polished and then oxidized in phosphoric or oxalic acid solution (Figure 5A,a). A two-dimensional array of cylindrical nanopores was obtained.^{48a,c} The diameter of the pores, which ranged from 15 to 150 nm, may be adjusted by varying the anodic voltage, the solution pH and composition, and the temperature during the formation of the AAO film. The parallel alignment of the AAO film ensures the formation of metal nanowires. Alternating current (AC) with a frequency of ~ 50 Hz was applied to deposit the metal into the pores (as shown in Figure 5A,b) with the voltage controlled from 2 to 20 V depending on the thickness of the barrier layer of the AAO film. Well-ordered metal nanowires with appropriate lengths were exposed on the surface by controlled etching of the surrounding alumina in dilute phosphoric acid (Figure 5A,c). Figure 5B–D shows AFM images of metal nanowires after the aluminum oxide was removed partially. It can be seen that two-dimensional arrays of nanowires were successfully fabricated by the AAO template synthesis method and the wires were parallel to each other and normal to the surface (Figure 5B). It is necessary to point out that, because the AFM tip is not sharp enough to go down to the bottom of the wire when the wire is longer than about 100 nm, the AFM images are distorted to some extent because the cone shape of the tip (Figure 5C). On increasing the dissolution time, the length of nanowires exposed on the surface increased. Finally the nanowires collapsed on the aluminum surface, and the length of the nanowires is more than 1 μ m, as shown in Figure 5D.

Figure 2e illustrates a good-quality SERS spectrum of pyridine adsorbed on a Ni nanowire with an average diameter of about 50 nm arrays fabricated by AC deposition. The SERS signals observed are stronger than from the conventionally roughened transition-metal electrode surfaces. It is worth noting that the SERS spectral features, including the frequency and relative band intensity, from the nanowires are nearly identical to those of bulk electrodes at the open circuit potentials. The SERS intensity depends critically on the length of the nanowires exposed at the surface and is considerably stronger than that from the normal roughened surfaces.^{48f,g} This shows that ordered nanorod arrays could serve as a new class of SERS-active substrates especially for transition metals.

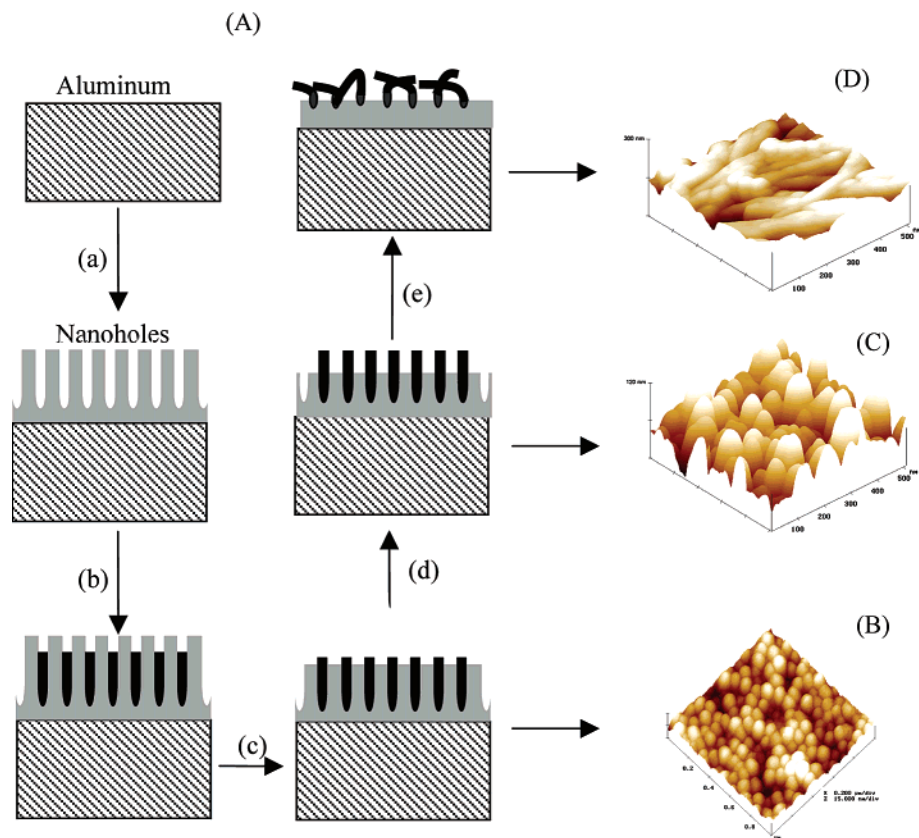


Figure 5. (A) Schematic diagram of the fabrication process of metal nanorod arrays. (a) Anodic oxidation, (b) alternative current deposition of metal, (c) dissolution of the AAO layer to the emergence of the metal nanorods, (d) partial dissolution of the AAO(anodic aluminum oxide) layer to the appearance sufficient length of nanorods while they are standing on the surface, and (e) collapse of the metal nanorods on the AAO surface. The corresponding AFM images at different stages of the dissolution of the AAO layer (B) at the initial stage, (C) at the intermediate stage with the nanorod having 100 nm protrusion over the surface, and (D) at the final stage after the collapse of the nanorods onto the surface.

3.1.6. Comparison with “Free-Electron” Metal Systems.

Table 1 is a summary of the typical experimental parameter that we have varied in the surface pretreatment of various metals. It can be seen that there are more than five methods to prepare SERS-active metal surfaces. It should be noted that some of the roughening procedures aforementioned are quite different from those employed for conventional SERS-active metals, Ag, Cu, and Au.^{1–5} For example, most of the roughening procedures for noble metals involve a Cl^- -containing solution, and the surface obtained is normally quite loose and could be removed by a slight touch of the fingers. The residual Cl^- could have effects on the surface adsorption or reaction process and, consequently, the resulting spectra.

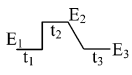
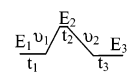
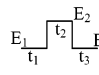
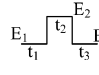
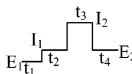
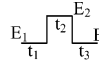
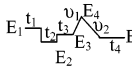
To obtain good SERS signals, an in situ ORC roughening procedure is generally used for Ag and Cu electrodes, so that problems of irreversibility and instability in the SERS measurements arise. In particular, at more negative potentials, adsorbates are desorbed, causing the decomposition of metastable adatoms (adclusters) with high SERS activity.^{5d,41} It inevitably leads to a sharp decrease or an irreversible loss in SERS intensity. The roughened transition metals show considerably better stability and reversibility. Pt shows the best stability following an extensive surface treatment after the ORC. The latter consists of potential cycling the freshly roughened Pt electrode between -0.25 to $+1.25$ V to remove all unstable particles and impurities. The cyclic voltammograms (Figure 3b) on the smooth Pt surface for general use and the roughened Pt present several similar characteristic regions.

A comparison of the reversibility of Pt and Ag electrodes after potential cycling is shown in Figure 6.⁵³ For the Ag

electrode, the signal suffers a substantial irreversible loss, whereas the Pt electrode has very good stability and reversibility. The surface Raman signal could be recovered almost completely on returning to a more positive potential following a very negative potential excursion. Hence, the Pt electrode can be reused for a long time as long as it is subjected to an electrochemical cleaning procedure, i.e., by cycling in a H_2SO_4 solution before each new experiment. Furthermore, we found that SERS from this surface is quite uniform from spot to spot. This ensures that the vibrational properties of the adsorbate probed by surface Raman spectroscopy are reasonably representative of the entire surface rather than some special SERS-active sites.

3.2. Calculation of the Surface Enhancement Factor (SEF) in a Confocal Microprobe Raman System. In our studies, we have found that the increase in the surface signal intensity is not simply proportional to the surface roughness factor (R) for various transition-metal surfaces; one should therefore consider the SERS effect. There is still controversy as to whether transition metals can exhibit SERS activity or not. It is highly desirable to clarify this question as we are now able to obtain good-quality Raman spectra from various transition-metal surfaces. We have proposed a method to accurately calculate the SEF after considering the special feature of the confocal Raman system.^{35c,36c} As in most SEF calculations, pyridine (Py) is employed as the model molecule and Pt is a typical transition metal; the Raman intensity of the total symmetric vibration (ν_1) of Py is used to calculate the SEF of the Pt surface. Only a brief description is given here; details can be found elsewhere.^{35c,36c}

TABLE 1: Surface Roughening Procedures for Various Metal Electrodes^a

	Pretreatment	Electrolyte	Potential waveform	Parameters	Cycles	Surface appear.
Ag	Chemical etching (optional)	0.1 M KCl		$E_1=E_3=-0.25$, $E_2=0.25$ $t_1=15, t_2=8, t_3=60$	1	Milky Yellow
Au	Electrochemical cleaning (optional)	0.1 M KCl		$E_1=E_3=-0.3$, $E_2=1.2$ $t_1=t_3=30$, $t_2=1.2$ $v_1=1$, $v_2=0.5$	25	Dark brown
Cu	Electrochemical cleaning (optional)	0.1 M KCl		$E_1=E_3=-0.4$, $E_2=0.4$ $t_1=15$, $t_2=3-5$ $t_3=60$	1-5	Dark brown
Pt	Electrochemical cleaning	0.5M H ₂ SO ₄		$E_1=E_3=-0.2$, $E_2=2.4$ $f=1.5$ ($t_1+t_2=1/f$)	30-900	Gray to dark yellow
Pt, Rh	Electrochemical cleaning	0.5M H ₂ SO ₄		Pt, $I_1=-I_2=1.6$, $f=0.5$ Rh, $I_1=-0.1$, $I_2=0.13$ $f=0.2$ ($f=t_2+t_3$) $E_1=E_2=-0.2$	10-600	Misty gray to dark brown
Fe	Chemical etching (optional)	0.5M H ₂ SO ₄		$E_1=E_3=-0.7$, $E_2=0.35V$ $t_1=t_3=60$, $t_2=15$	1	Gray
Co	Chemical etching (optional)	0.5 M NaClO ₄		$E_1=-1.0$, $E_2=-1.4$, $E_3=-1.2$, $E_4=1.0$, $E_5=-1.25$, $t_1=t_3=20$, $t_2=15$, $t_4=60$, $v_1=0.2$, $v_2=0.1$	1	Dark

^a Units: E (V), t (s), I (A/cm²), v (V/s), and f (kHz).

The SEF(G) is defined as the ratio of the integrated intensities contributed by the molecules on the surface and in the solution, respectively.^{2,4,41} Thus

$$G = \frac{I_{\text{surf}}/N_{\text{surf}}}{I_{\text{bulk}}/N_{\text{bulk}}} \quad (2)$$

where I_{surf} and I_{bulk} denote the integrated intensities for the ν_1 mode of adsorbed pyridine, Py_{ads}, and pyridine in solution, Py_{sol}, respectively, whereas N_{surf} and N_{bulk} represent the number of corresponding Py_{ads} and Py_{sol} molecules excited by the laser beam. The N_{surf} can be calculated using the following approximation:

$$N_{\text{surf}} = \frac{R\pi a^2}{\sigma} \quad (3)$$

where R is the roughness factor of a Pt electrode, and a is the radius of the laser focal spot. Thus, $\pi a^2 R$ gives the total surface area occupied by the adsorbates, whereas σ is the surface area occupied by an adsorbate. In eq 2, the only unknown parameter is N_{bulk} . Because the confocal Raman microscope possesses a very good depth resolution, the collection efficiency for scattered

photons from pyridine molecules in each plane of the solution varies with the confocal depth. N_{bulk} cannot be obtained by a method based on the conventional Raman spectrometer. It should be calculated based on the special confocal feature of the microscope. We have found that the vertical spatial resolution of the confocal system with the same pinhole and slit size for the same objective is quite different with and without the water overlayer. Therefore, the number of pyridine molecules in the aqueous solution effectively illuminated, N_{bulk} , can be written as

$$N_{\text{bulk}} = \pi a^2 h c N_A \quad (4)$$

where c is the concentration of solution species, N_A is Avogadro constant; h (in units of μm), which is the key parameter of the confocal characteristic, depends on the pinhole size and the magnification of the objective of the Raman instrument and decreases with decreasing pinhole size. Substituting N_{bulk} and N_{surf} from eqs 4 and 3 in eq 2 gives

$$G = \frac{c N_A \sigma h I_{\text{surf}}}{R I_{\text{bulk}}} \quad (5)$$

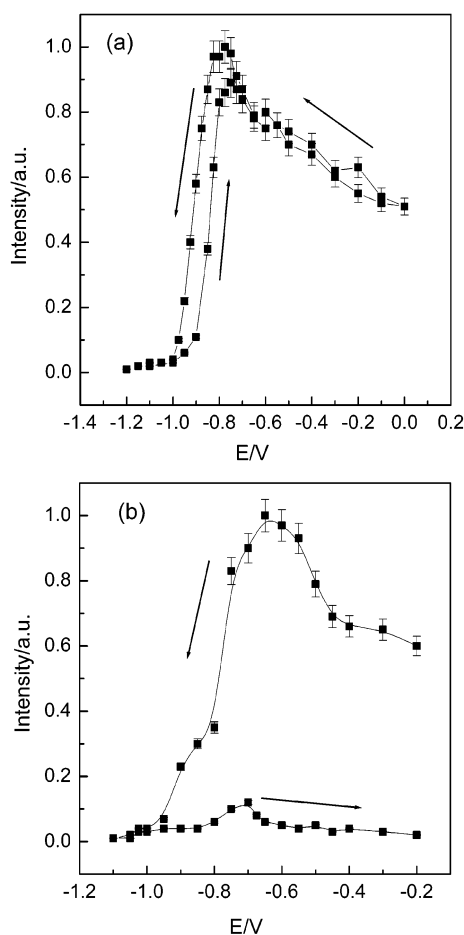


Figure 6. Integrated intensity–potential profile for ring breathing mode ν_1 of adsorbed pyridine on Pt (a) and Ag (b) surfaces showing the SERS reversibility of different SERS substrates. Solution: 0.01 M pyridine + 0.1 M NaClO₄.

Thus, from the surface Raman signal detected, the solution spectrum, and the solution concentration, we can calculate the SEF for different electrode materials.

Using Py as the probe molecule and the 632.8 nm line of a He–Ne laser excitation, we obtained the SEFs of five roughened transition metals Fe, Co, Ni, Rh, and Pt, whose maximum SEFs that have been obtained are 2000, 1000, 1000, 5000, and 2000, respectively, by comparing to the value of about 10^6 for Ag under the same measurement condition. Besides the difference in the nature of the metals, the actual SEF value for the same metal depends on the method of surface pretreatment. It is necessary to point out that the SEF value depends also on the probe molecule and the exciting line. By improving the surface pretreatment and choosing an appropriate excitation line, the SEF could be increased. The correct calculation of the SEF is important for a study of the SERS mechanism (vide infra) and helpful for SERS applications. In the following, we will give some examples of practical applications of SERS in order to demonstrate the power and potential of Raman spectroscopy as a surface spectroscopic tool.

TABLE 2: Adsorbates on Transition Metals Studied by SERS

metal	adsorbates				
Pt	pyridine	benzene benzonitrile	thiourea	H, CO	CN [−] SCN [−] Cl [−] , Br [−]
Rh	pyridine	benzene	H	CO	
Fe	pyridine pyrazine	benzotriazole benzonitrile	SCN [−]		
Co	pyridine	benzotriazole benzonitrile	SCN [−]		
Ni	pyridine	pyrazine	SCN [−]	N ₃ [−]	
Pt–Rh, Pt–Ru Pt–Ir	pyridine	CO			
Ru, Pd	pyridine				

3.3. SERS Applications in Transition-Metal-Based Systems. During the past six years, with the help of the highly sensitive confocal Raman microscope and the development of special surface preparation methods, our group has extended SERS studies of various molecule and ions adsorbed on transition metals (Table 2).

We will restrict ourselves to some representative examples: (1) pyridine adsorption on various transition-metal surfaces as the model system for SERS study, (2) Br[−] adsorbed on Pt, to illustrate adsorbate–substrate interaction as well as competitive and parallel adsorption of difference species, (3) dissociative adsorption of methanol on bimetallic electrodes, and (4) the inhibition effect of benzotriazole on Fe corrosion. The latter two are of importance in the areas of fuel cell and corrosion.

3.3.1. Surface Raman Scattering of Pyridine from Transition-Metal Surfaces. Good-quality surface Raman spectra of pyridine, adsorbed at Pt, Ni, Ru, Rh, Pd, Co, and Fe electrodes in a very wide electrode potential region (e.g., −1.0 V to +1.4 V), have been obtained. It is of interest to have a deeper insight into SERS phenomenon by comparing the spectra of pyridine on transition metals with that on the “free electron” metals Ag, Au, and Cu and from the liquid, as shown in Figure 7a. The spectra from different metals are selected at their potentials where the SERS intensity reaches the maximum value. The four major bands located at about 630, 1010, 1215, and 1595 cm^{−1} are attributed to the ring in-plane deformation (ν_{6a}), ring breathing (ν_1), C–H in-plane deformation (ν_{9a}), and ring stretching (ν_{8a}) vibration, respectively.^{2,54} We have found that the SERS spectra distinctively depend on the nature of the substrate. Several key features should be noted from these metal-dependent spectra: (i) the wavenumber of the ν_1 band changed from 1001 cm^{−1} on Pd to 1015 cm^{−1} on Pt at the same potential of −0.6 V, (ii) the frequency–potential profiles of transition metals are quite similar to those of Cu and Au but rather different from Ag, see Figure 7b, (iii) the potential where the intensity reached its maximum value varied from −0.6 for Pt to −1.5 V for Fe, and (iv) the relative intensities of the four bands, e.g., the intensity ratio of the ν_1 to ν_{9a} , varied from 3.0 for Pt to 0.67 for Co. These features could be attributed to substantially different adsorption behavior of pyridine on different surfaces.^{27b,37}

Although pyridine is the most widely used model molecule for SERS, a quantitative explanation for the remarkable spectral differences on different metal surfaces is still lacking even for the three noble metals. So far, people have not been able to interpret comprehensively the spectral features, such as the changes in intensity and frequency for the different metals. An example is the distinctive differences in the intensity of the ν_{12} band at about 1035 cm^{−1}, which is the second strongest band for pyridine in the liquid and gas phases. This band has very high intensity on Ag but very weak on Au and Cu. We can find no satisfactory explanation in the literature to interpret this substrate-dependent spectral feature. It is even more surprising that this band almost vanishes on most of the transition-metal surfaces as shown in Figure 7. It indicates that the chemisorption interaction can enhance the Raman scattering cross section of

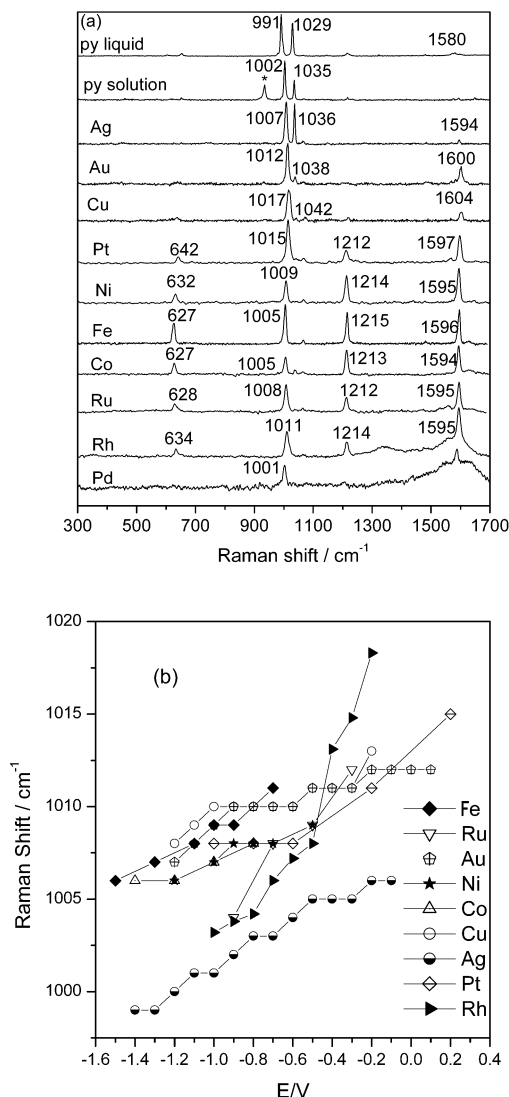


Figure 7. (a) Raman spectra of pure pyridine, pyridine solution, and pyridine adsorbed on noble metal and transition metal surfaces at open circuit potentials and (b) the dependence of the frequencies of the ν_1 vibration of selected metal on the electrode potential. (*) The band at 932 cm^{-1} is the total symmetric stretching vibration of ClO_4^- in the bulk solution. The exciting wavelength: 632.8 nm .

some vibrational modes or reduce some. It seems to be necessary to reinvestigate this model system at a more basic level, i.e., through quantum chemical calculations. It appears to be a timely undertaking because we have now obtained abundant experimental data from various transition metals for the detailed comparative theoretical study.

We have used density functional theory at the level of B3LYP/6-311+G** (for C,N,H)/LanL2DZ (for metals) for normal coordinate calculations of the neutral and cationic species of the pyridine–metal atom (ion) complexes that simulate the electrode surface at open circuit potential or with a negative charge. New assignments of the fundamental frequencies for the bands attributed to the ν_{17a} , ν_3 , ν_5 , and ν_{18b} modes of the free pyridine in the reported Raman spectra have been suggested. The calculated results are in good agreement with the experimental results for both transition metals and noble metals. The calculated frequency shifts indicate that the coupling of ν_1 , ν_{12} , and ν_{18a} modes depends on the strength of the N–metal bond and its bonding properties. Potential energy distribution (PED) of the ν_{12} mode varies substantially for different metals with different Fermi level. It also indicates that the PEDs should be

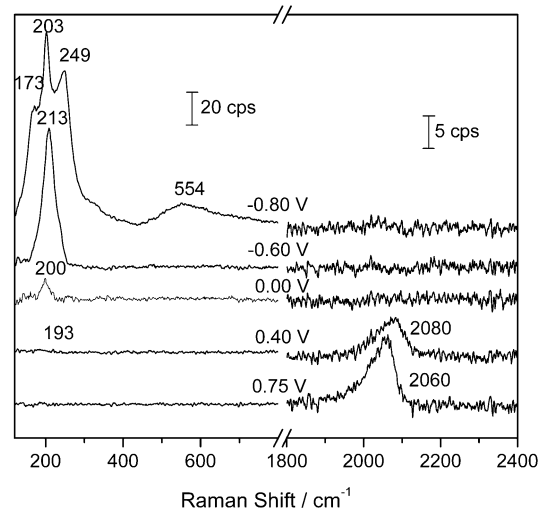


Figure 8. Potential-dependent surface Raman spectra of competitive adsorption of bromide and hydrogen at a platinum electrode in a 1.0 M NaBr solution with $\text{pH} = 1$. The exciting wavelength: 514.5 nm .

different for the pyridine in the liquid and adsorbed on the metals except Ag that interacts most weakly with pyridine. The frequency of the ring breathing mode ν_1 is sensitive to the structural change associate with the weak σ donation and the large σ/π back donation. It is particularly interesting that the frequency of the ν_{6a} mode has a nearly linear relationship with the change of the force constant of the N–M bond. Hence, the frequency shift of ν_{6a} directly reflects the strength of the interaction of pyridine with the metal electrode under potential control. This analysis, together with the mechanistic study discussed in the next section, shows that, in order to fully utilize SERS for investigation of surface adsorption, it is also essential to make use of quantum chemistry.

3.3.2. SERS Studies on Surface–Adsorbate Interactions.

It would be useful to extend SERS of transition metals to the study of more general adsorbates and important organic and inorganic molecules having smaller Raman scattering cross sections. It is also of importance to pay special attention to vibrational bands in the low-frequency region below 400 cm^{-1} in order to gain insight into the nature of the metal–adsorbate bonding. Two fundamental problems in surface electrochemistry are the interaction of electrode surfaces with halide ions and hydrogen; the adsorption of these species plays a significant role in determining many other surface processes.⁵⁵ Pt is one of the most investigated metals that shows strong interaction with halide ions and hydrogen.⁵⁶ Figure 8 shows the Raman spectra of bromide and hydrogen competitively adsorbed at a Pt electrode over a wide potential region. At potentials negative of 0 V , the band located in the frequency region from 2060 cm^{-1} is attributed to the adsorption of a hydrogen atom singly coordinated on top of a surface Pt atom. At 0 V , a vibrational band due to Pt–Br at ca. 200 cm^{-1} was detected, whereas the Pt–H band disappeared, indicating that the hydrogen is replaced by Br^- on the surface. This band increased in intensity and frequency with a positive shift of potential. A more significant change was detected at potentials positive of 0.6 V , where the oxidation of Pt occurred (the 554 cm^{-1} band is attributed to the Pt–O vibration). The emergence of bands at 249 , 203 , and 173 cm^{-1} , which correspond to the stretching and bending vibration modes of $\text{Br}-\text{Br}$ in Br_3^- ,⁵⁷ provide clear evidence for the formation of Br_3^- on the oxidized surface. These preliminary results demonstrate the virtues of surface Raman spectroscopy for yielding information on surface bonding

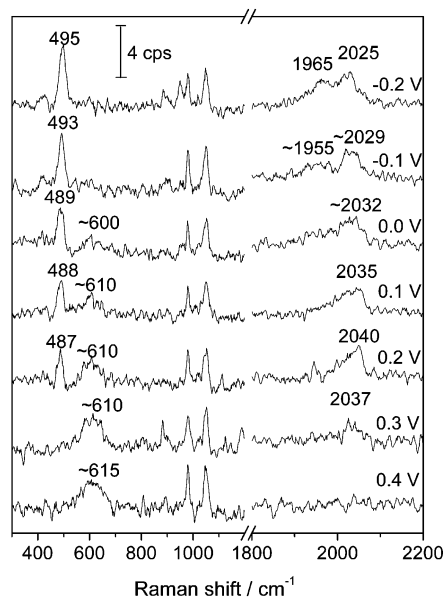


Figure 9. Surface Raman spectra of a roughened Pt electrode covered with underpotential-deposited Ru ($\theta_{\text{Ru}} = 0.7$) in 0.1 M CH_3OH + 0.1 M H_2SO_4 . The excitation line: 632.8 nm.

as a result of surface coverage, coadsorbate, and electrode potential.

3.3.3. Dissociative Adsorption and Oxidation of Methanol on Pt–Ru Electrodes. The advantage of SERS in the study of surface bonding can be further demonstrated in some more practical systems. From the viewpoint of electrocatalysis, we have chosen a system related to fuel cells.⁵⁸ We have studied dissociative adsorption and oxidation of methanol at Pt–Ru electrodes with different surface roughness in sulfuric acid solutions.⁵⁹ The activity of Pt–Ru toward the oxidation of methanol is significantly higher than that of Pt alone, indicating that alloying with Ru promotes the oxidation of methanol. Among the mechanisms proposed to interpret the promotion by Ru is the bifunctional mechanism which has been supported by a number of electrochemical evidences.^{55,60} Because oxygen-containing species can adsorb on the Ru surface at a potential which is about 0.2–0.3 V lower than that on the Pt surface, it facilitates the oxidation of hydrocarbon to CO_2 at a lower potential. Taking advantage of the ability of Raman spectroscopy to obtain vibrational information in the low-frequency region, an experiment was done to obtain direct evidence for the bifunctional mechanism.

Figure 9 shows potential-dependent surface Raman spectra obtained on a roughened Pt–Ru ($\theta_{\text{Ru}} = 0.7$) electrode in a 0.1 M sulfuric acid solution. Carbon monoxide (CO), widely presumed to be the poisoning intermediate in the dissociative adsorption of methanol, was detected in a wide potential range appearing as a broad band at 2045–2053 cm^{-1} . A shoulder on the low-frequency side of the 2025 cm^{-1} peak was assigned to CO adsorbed onto the Ru surface. This peak became more obvious when the electrode potential was more negative than -0.1 V, which can also be verified by the appearance of the Pt–(Ru)C band at 490 cm^{-1} . It should be noted that a broad band at 600 cm^{-1} appeared at 0 V, which increased with a more positive potential. Under the same conditions, no discernible signal could be detected on a pure Pt electrode. The oxides on Pt can only be observed when the potential is more positive than 0.7 V. Therefore, it is reasonable to assign the band at 600 cm^{-1} to an adsorbed oxygen-containing species on the Ru surface. The more oxygen-containing species exist on the surface, the easier the CO band can be oxidized to CO_2 . This is

in good agreement with results obtained from electrochemical studies, in which it was found that the adsorbed oxygen species appears at 0 V.⁵⁹ The results also show that the confocal Raman microscope is a useful tool for the in situ study of highly rough electrodes, with dark color, which are commonly used in practical catalysis.

3.3.4. Inhibition of Benzotriazole on Fe Corrosion. Iron is one of the most important and widely used metals. The corrosion and passivation of iron are quite general and important phenomena in industry. Therefore, there is great economic incentive in developing methods and materials to alleviate corrosion.⁶¹ This comes only from a good understanding of the mechanisms and processes involved in this complex phenomenon. It is well-known that benzotriazole (BTAH) is an effective inhibitor for Fe corrosion.^{62,63} On the other hand, the addition of I^- in the solution will hinder the anodic process, resulting in the positive movement of the corrosion potential. However, if benzotriazole and I^- are added together into the system, the inhibition effect becomes remarkable, indicating the existence of a synergetic effect of I^- and benzotriazole. It will be very helpful to obtain the information reflecting the interaction between the anion and the organic molecule as well as their interaction with the surface by Raman spectroscopy.

Figure 10a presents SERS spectra of BTAH adsorbed on the Fe surface in solutions containing I^- of different concentration. For the convenience of comparison, all of the spectra were acquired at -0.5 V, and the peaks at 979 and 1052 cm^{-1} are from the vibrations of SO_4^{2-} and HSO_4^- of the bulk solution, respectively. The spectral feature from the surface species demonstrates the characteristic vibrations of the neutral and protonated form of BTAH (BTAH_2^+).^{63a} All of the intensities of the bands related to BTAH decrease with the addition of I^- . Furthermore, the higher the I^- concentration is, the lower the intensities of the BTAH bands will be. When the I^- concentration is higher than 10^{-3} M, no surface signal from BTAH can be detected. Accordingly, one can conclude that the solution containing I^- , BTAH, or BTAH_2^+ is replaced by the adsorbed I^- at the surface. There is no direct interaction between the Fe surface and BTAH or BTAH_2^+ . However, because of the formation of the adsorbed layer, BTAH_2^+ can adsorb more easily on the surface by electrostatic interaction. The synergetic effect of both species results in the improvement in the inhibition efficiency. To interpret the synergetic effect, we performed SERS and electrochemical studies systematically on Fe in solutions containing different electrolyte and proposed three adsorption models accordingly as shown in Figure 10B–D.⁶³

The above four studies show remarkable advantages of SERS study on some fundamental or practical systems. It is particularly important that practical catalysts and porous electrodes can be in situ investigated under truly catalytic and electrochemical condition. The wide variety of samples even deeply dark in color and highly rough in morphology can be studied by SERS, which are difficult or even impossible to be accessible by many other spectroscopic techniques.

4. Enhancement Mechanism of Transition Metals

The SERS mechanism is always an important issue in the SERS field and has attracted much interest from various communities of surface science, spectroscopy, condense-phase physics, and nanoscience.^{4,12–15,64–68} After obtaining SERS from transition-metal systems and calculating the enhancement factors based on the experimental data, naturally, we have tried to figure out microscopically the origin of SERS from transition metals that have not generally been considered as effective SERS

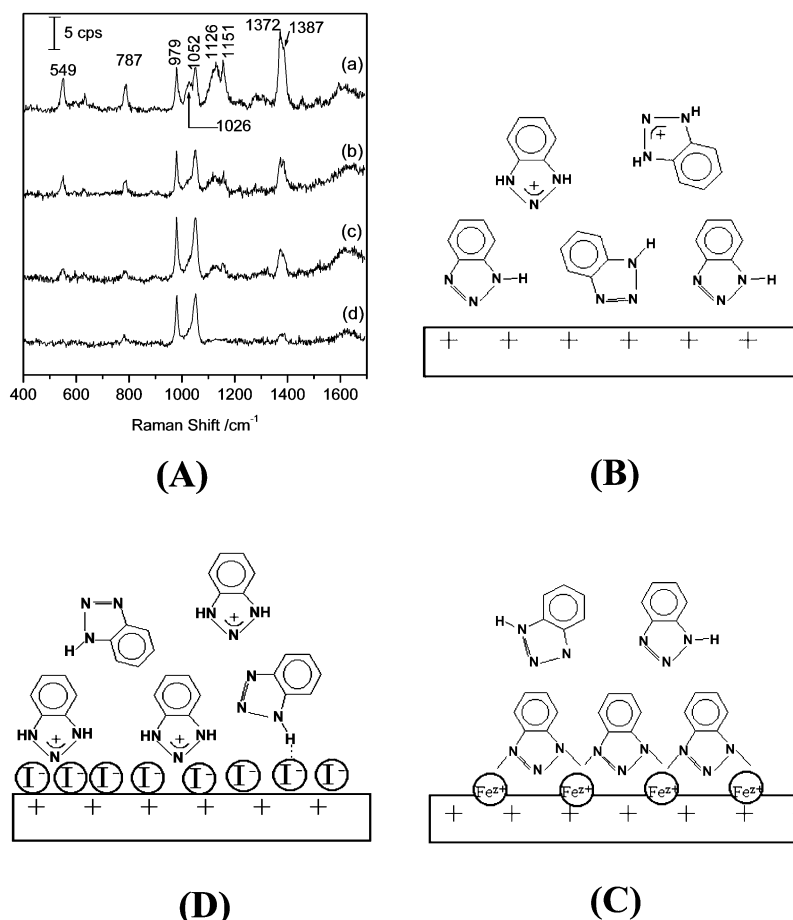


Figure 10. (A) Surface Raman spectra of BTAH adsorbed on the Fe surface in 0.5 M H₂SO₄ at -0.5 V (a) without KI and with (b) 1×10^{-4} M KI, (c) 5×10^{-4} M KI, and (d) 1×10^{-3} M KI. The exciting wavelength: 632.8 nm. The model proposed for the adsorption configuration of BTAH on an iron electrode with positive charge in the (B) acidic solution, (C) neutral solution, and (D) acidic solution containing I⁻.

substrates. On the basis of our experimental results correlated with surface roughness at the nanometer scale, such as that the SERS intensity depends apparently on the surface protrusion of the nanorod arrays,^{48f} we strongly believe the existence of the EM enhancement. On the other hand, the excitation wavelength dependence of the intensity-potential profile observed in some SERS systems^{36c,37c,e} (vide infra) gives strong evidence that the chemical enhancement is cooperative as well in these systems. For a better description of the contribution of both SERS mechanisms, the SERS intensity is approximately expressed by several groups as^{13,14}

$$I_{\text{SERS}} \propto |E_{\text{Surf}}/E_{\text{Light}}|^2 |E_{\text{S}}/E_{\text{s}}|^2 \sum_{\rho, \sigma} |(\alpha_{\rho\sigma})_{nm}|^2 \quad (6)$$

where E_{Surf} , E_{Light} , E_{S} , and E_{s} are electromagnetic (optical electric) fields of the surface and the incident lights and that of the scattered light of the surface molecule and the free molecule, respectively. The incident radiation results in large local fields at the properly roughened surface. It increases remarkably the Raman scattering intensity of the surface species, which is proportional to the square of the surface local electric field. The rough surface not only enhances the incident laser field but also the Raman scattered field;^{14,68} therefore, the product of the $|E_{\text{Surf}}/E_{\text{Light}}|^2 |E_{\text{S}}/E_{\text{s}}|^2$ determines the total EM enhancement factor, contributed by the incident light and the scattered light. The sum term of $(\alpha_{\rho\sigma})_{nm}$ describes the optical response of the intramolecular interaction and the interaction between the molecule and the metal surface, resulting in the chemical enhancement.

In general, the EM enhancement is determined by the interaction of (incident and scattered) light and metal, which depends critically on the wavelength of the exciting light, the optical electronic property of metal, and the surface morphology. From these different aspects, the EM enhancement includes several processes, such as the surface plasma resonance, lightning-rod effect, and collective effect of the particle aggregate.^{4,9,10,12,14,65,68} The chemical enhancement is contributed by the chemisorption interaction and the photon-driven charge transfer between adsorbates and substrates.^{4,13,15,67e,68} We think that the SERS mechanism of the noble metal can be extended, in principle, to apply to the transition metal. Accordingly, on the basis of the previous theoretical works,^{12,13,65–68} we have carried out a comparable study on transition metals and noble metals theoretically and experimentally in the aspect of SERS mechanism.

4.1. EM Enhancement. The electromagnetic field enhancement of the noble metal is considered to mainly come from a geometrically defined surface plasmon resonance at metal nanoparticles.^{4,12,14,65,66} The electromagnetic field of the light at the surface can be greatly enhanced under conditions of surface plasmon resonance (collective electron resonance) for “free-electron” metals.^{65,66} All metals including transition metals can enhance to a greater or lesser extent so that the EM part of the contribution to the enhancement depends on the metal’s ability to sustain surface plasmons of high resonance quality. In comparison with the noble metals and alkali metals, transition metals have very different electronic structures, where the Fermi level locates at the d band and the interband excitation occurs

very possibly in the visible light region.⁶⁹ The coupling between conduction electrons and interband electronic transitions depresses the quality of the surface plasmon resonance of transition metals considerably.¹³ Therefore, it reduces the effectiveness to show intense SERS, as observed in many experiments.

However, the electromagnetic field lying near high-curvature points on the rough surface should be carefully considered; for example, the lightning-rod effect^{65a} can result in a largest electric field near the sharpest surface of the needlelike rod. As a consequence, the maximum enhancement reaches at the spheroid tip and the field strength increases with the aspect ratio.²⁸ Accordingly, the lightning-rod effect may play the more important role to the EM enhancement for transition metals. The AFM images of the rough transition metal surfaces show that the surfaces with SERS activity all contain the aggregation of nanoparticles within the range of 50–150 nm.^{37e} On the basis of the previous theoretical calculation for the EM mechanism of the noble metal,^{65a,b} we used a model of a prolate hemispheroid of transition-metal protruding on a flat plane to calculate the local optical electric field contributing to the SERS. In this preliminary study, we only considered an isolated Co particle as a simple model without taking into account the coupling between particles. Actually, the effect of the interparticle coupling is important in understanding the EM mechanism of the metal nanoparticle aggregates.^{12c,42} Nevertheless, the calculated result indicates that the Raman signal depends on the shape and the size of the prolate and the dielectric constant of the metal and the ambient medium, as shown in Figure 11. The EM enhancement factor of a vibrational mode with the dipole moment along the *z* axis changes with the exciting photon energies. When the optical dielectric constant of 1.77 for water was adopted,^{28,68a} the changes of the EM enhancement factor are shown in Figure 11. It is well-known that the SERS enhancement factor of the noble metal increases sharply when the frequency of the excitation light is close to the frequency of the surface plasma.^{14a,e} In contrast, the curves obtained from the transition metal are much broader, as seen in Figure 11. It implies that the enhancement factor of the transition metal is relatively small and does not critically depend on the excitation line. Because the most efficient enhancement occurs along the semimajor axis of the prolate spheroid, a factor of $\sim 1/17$ for scaling the top enhancement was used to obtain the average effect for the whole particle.^{68a} Accordingly, the average EM enhancement factor of ~ 100 fold is reasonable at the excitation lines of 514.5 and 632.8 nm to interpret the EM enhanced mechanism of the rough Co electrode. This value is similar to the electrodynamics calculation on spheroids of Pt, Rh, Ni, and Pd by Chang and co-workers.²⁸

Figure 11b shows that the enhancement increases with the increase of the aspect ratio remarkably. The nanowire array could be more suitable for studying the lightning-rod effect as we have found that the SERS intensity depends critically on the length of nanowires exposed on the substrate surface. The exposed length was controlled by varying the etching time of the AAO template, as shown in Figure 5. The SERS intensity increased quickly at the beginning and decreased suddenly after some etching time.^{48g} The maximum intensity is about twenty times as strong as that at the initial stages of the etching process. There is no doubt that the increase in intensity is partially due to the increase of the surface concentration of the adsorbate when the longer wires were exposed to the solution. However, it cannot explain the significant quenching in SERS intensity in the final etching process when the exposed surface area of nanowires might increase to the maximum. It is also very hard

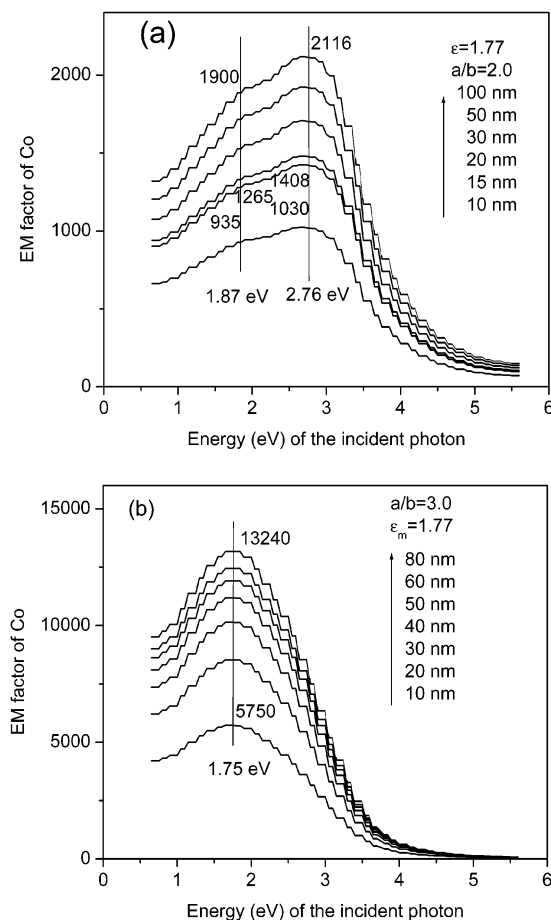


Figure 11. Changes of the EM enhancement factors by evaluating a polarize dipole located at the tip of hemispheroid with the aspect ratio, a/b on a conduction planar plane. (a) $a/b = 2$, $\epsilon_m = 1.77$; (b) $a/b = 3$, $\epsilon_m = 1.77$. This dipole system is the ring-breathing mode of pyridine, which has a vibrational frequency of 1008 cm^{-1} .

to be explained in terms of the chemical mechanism because the number of SERS active sites is proportional to the surface area. Therefore, the major contribution to the dependence of intensity on the etching time is due to the EM enhancement; that is, the electric field at the end of the wire reached its maximum under the favorable length.

It is necessary to point out that the theoretical consideration on the transition metal is based on the previous works on the noble metals, and the model of the single nanospheroid is very simple. Recent advances in theory can evaluate the optical response of particles with various shapes for an arbitrary rough surface.^{42f,65e,70,71} The discrete dipole approximation (DDA) is one of powerful methods.⁷² However, at the present stage, DDA have not been able to apply to transition-metal system because their refractive index ($|m - 1| > 3$) is larger than what is used for the DDA method. It is therefore a challenge to further extend this method to study a variety of transition-metal surfaces.

More importantly, our preliminary study neglected the role of interparticle interactions that are known to result in the very intense enhancement at interstitial sites of small clusters and in a more complicated pattern of hot spots in larger random metal clusters.^{40b,42,71} Indeed, a consensus now exists, largely as a result of the work of Kall and co-workers^{40a,b} and Brus and co-workers^{40c,d} that hot sites in small interacting aggregates are essential in producing the very large enhancements observed in single molecule SERS.^{38–40} In fact, the theories of Metiu^{14b,65c,d}

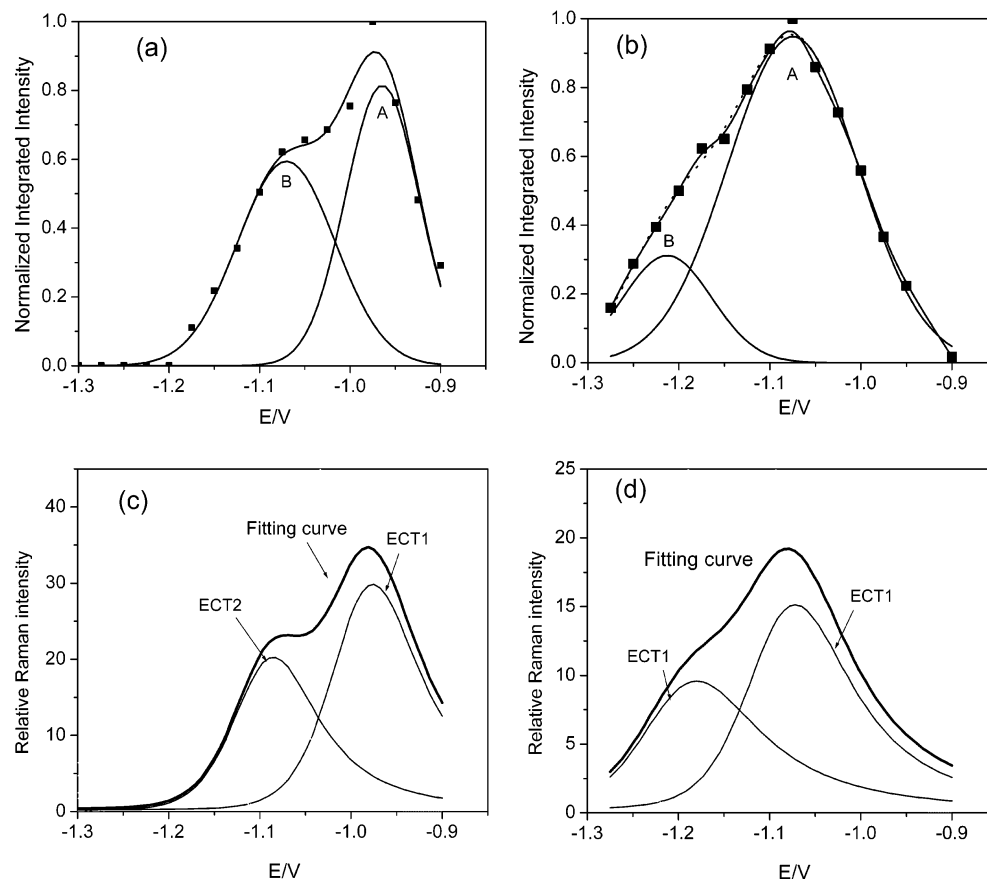


Figure 12. Normalization Raman intensity–potential profiles and their simulation curves for pyridine adsorbed on a rough cobalt electrode. The contributions from the vibrational excited states ($\nu = 0, 1$, and 2) of the two excited charge-transfer states are considered. (a) The excitation line of 514.5 nm. (b) The excitation line of 632.8 nm for another substrate sample. (c) The excitation line used is 514.5 nm. $\Gamma_1 = 0.27$ eV, $\Gamma_2 = 0.27$ eV; $TD_1 = 3.80$ D, $TD_2 = 3.42$ D. (d) The excitation line used is 632.8 nm. $\Gamma_1 = 0.34$ eV, $\Gamma_2 = 0.40$ eV; $TD_1 = 3.80$ D, $TD_2 = 3.78$ D.

and Nitzan^{65a} and others dating from the early 1980s predicted such effects and more recent calculations by Kall and co-workers^{38d} and Martin and co-workers.^{66b–d} Along with this direction, a more comprehensive theory will be applied not only for noble metals but also for transition metals.

4.2. Chemical Enhancement. Owing to the chemisorption interaction, the Raman scattering cross section of the vibrational modes in the adsorbate can be enhanced under certain condition, such as orientation change.⁶⁸ As has been pointed out above, the interaction can lead to the increase or decrease in intensity for different modes of pyridine as shown in Figure 7. Therefore, we need to keep in mind that when the molecule adsorbs on the metal surface the change in the electron distribution of molecule even under its electronic ground state may cause different enhancements for different vibrational modes.

The photon-driven charge-transfer enhancement is a well-known mechanism as a resonance-like Raman enhancement.^{13,15,67,68} This complex mechanism is associated with the excited state of the molecule/metal system and with the charge transfer between the molecule and the metal surface (or adatom and adclusters).^{4,13} The photon-driven charge-transfer mechanism can be easily verified by obtaining the intensity–potential profile with the changing exciting line (incident photon energy). Taking pyridine adsorbed on a metal surface as an example, the contribution arises from the ground-state charge transfer.⁷³ Following the previous works on the noble metals,^{15,67} we have recorded the intensity–potential profiles from various transition metals.^{36c,37c–e} Here, we take the ring-breathing mode of the pyridine adsorbed Co,⁷⁴ see Figure 12, and Pt^{36c} as an example.

As the exciting line changes from 514.5 to 632.8 nm, the peak potential moves to a more negative potential. The difference in the peak potential of the two profiles is about 130 mV for Co^{74b} and 200 mV for Pt.^{36c} In this case, the charge-transfer happens from the metal to pyridine.

A parameter S has been proposed by Kudelski and Bukowska to describe the dependence of the potential shift on the exciting frequency ν .^{75a} Accordingly, for pyridine adsorbed on noble metal electrodes, the S of different values have been reported, about 1.85 eV/V for Cu,^{75b} 2.26 eV/V for Ag,⁷⁶ and 0.91 eV/V for Au.^{75a} The intensity–potential profiles in Figure 12 show that the S values are about 3.46 eV/V for Co and 2.25 eV/V for Pt.^{36c} The results indicate that the electrons on the Co electrode are more sensitive to the change of the electrode potential compared to other metals. It is of special interest to observe two peaks in the profile that are probably attributed to the formation of two excited charge-transfer states.^{78a} They are very likely arisen from the excitation of the 4s orbital to the mixing orbital of the metal 4p_x and π -typical 3b₁ orbitals of pyridine and the excitation of the 3d orbital to the π -typical 2a₂ orbital of pyridine, respectively.^{78b} On the basis of the intensity–potential profiles of the pyridine/Co system, the energy positions of the unoccupied orbitals were determined at about $-1.65 \sim -1.74$ eV and $-1.19 \sim -1.31$ eV for the affinity levels corresponding to the first and the second charge-transfer states below the vacuum level, respectively. A comparison of the unoccupied levels 3b₁ (π^*) and 2a₂ (π^*) (0.62 and 1.14 eV⁷⁷) of the free pyridine with that of the adsorbed pyridine shows that the unoccupied orbital energies lower when the adsorbate

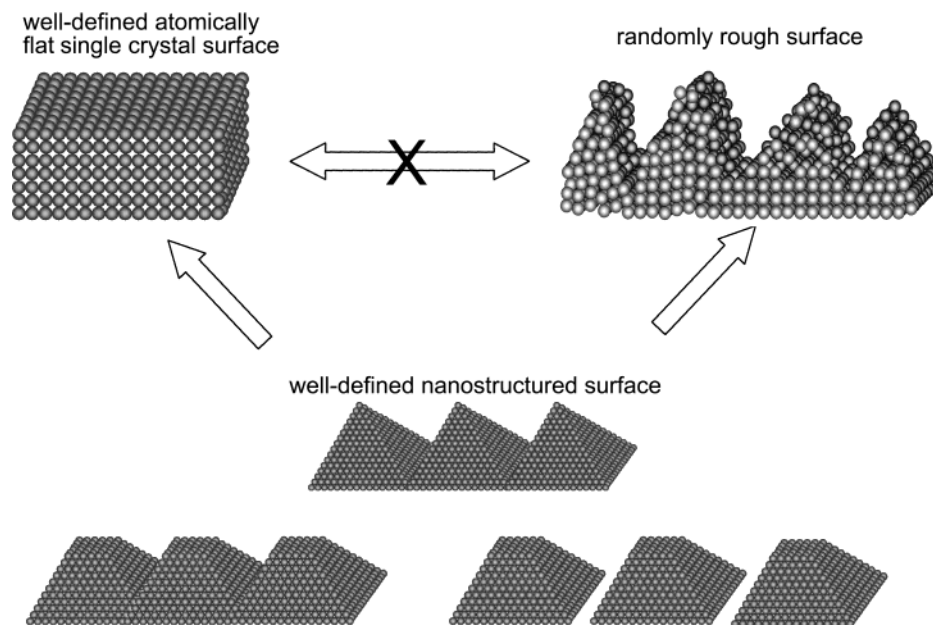


Figure 13. Schematic illustration of structures of a flat well-defined single crystal surface, a randomly rough surface, and a well-defined nanostructured surface precisely prepared to have well-defined surface facet and well-controlled space between each other.

interacts with the metal.⁷⁸ To explain the above experimental result, we performed the time-dependent density functional theoretical calculation.^{78b} The orbital energies for $3b_1$ and $2a_2$ orbitals are lowered to -1.75 eV and -1.19 eV, and the transition dipole moment is about 3.71 D (x) for the 2B_2 excited state for the initial state 2A_2 of the pyridine–Co complex.

The photon-driven charge transfer state is the intermediate state of the surface Raman scattering process. On the basis of the Fermi golden rule, the contribution from the CT state to the SERS cross section of the ring-breathing mode was calculated by the formulizm of the Kramers–Heisenberg–Dirac dispersion equation.⁷⁹ For the ν_1 vibrational mode of pyridine adsorbed at the Co surface, under the Condon approximation, the resonance Raman polarizability tensor can be written as^{40d}

$$\alpha_{\rho\rho} = \sum_k \frac{M_\rho^2 \langle f|k\rangle \langle k|i\rangle}{E_0 + \epsilon_k - \epsilon_i - \hbar\omega_i - i\Gamma} \quad (7)$$

where M_ρ is the transition dipole moment along the ρ direction. E_0 is the energy difference between the excited and ground electronic states. ϵ_i and ϵ_k are the vibrational energies of the electronic ground and excited states, respectively. Γ is the homogeneous line width of the excited charge transfer states. The initial value of the damping constant of the pyridine/Co system is selected to be $\Gamma = 0.40$ eV, which approaches to the half widths of the intensity-potential profiles, see Figure 13. The Franck–Condon factor $\langle f|k\rangle \langle k|i\rangle$ for Raman scattering process can be calculated according to that reported in the literature.⁸⁰ In the present system, the Franck–Condon factors are large from the vibrational quanta k of 0–2 in the excited state. Because there are differences in the electronic structures and the Raman scattering processes between the pyridine–metal surface and the cobalt–pyridine complex, it is necessary to further optimized the transition dipole moments, the damping constants and the energies of the both excited CT states. The calculated result is shown in Figure 12 parts c and d, which fits the experimental result quite well.

The chemical enhancement factor can be estimated by the ratio of the resonance Raman scattering intensity arising from

both the CT states of pyridine adsorbed on the surface and the normal Raman scattering intensity of the free pyridine molecule.^{15a,49b} The derivative of the polarizability along the ring-breathing mode is predicted about $24.36 \text{ \AA}^4/\text{amu}$ by the density functional calculation (B3LYP/6-31+G** (C, N, H)). Due to the fundamental frequency only being considered here, $\nu_1 = 1$ and then $2b^2 = 0.033 \text{ \AA}^2 \text{ amu}$. Thus, we obtained that the denominator in the above equation is 0.81 \AA^6 . From the curve in Figure 12, we can obtain that the total contributions from both excited CT states are 34.77 and 22.95 \AA^6 at -0.98 and -1.08 V, respectively. Hence, the enhancement factors for the exciting line of 514.5 nm are about 43 and 28-fold for the above two potentials, respectively. On the other hand, for the exciting line of 632.8 nm, the enhancement factors are about 24 and 15-fold at -1.08 and -1.18 V, respectively. Therefore, for the Co electrode, there is about 1 order of magnitude from the chemical enhancement of the adsorbed pyridine, whereas the surface averaging EM enhancement factor is about two orders.

It should be noted that many molecules and ions adsorb much strongly at the transition metal surfaces in comparison with the noble metal systems. When the strong chemical bond is formed, this chemisorption not only changes the electronic structure of adsorbate itself but also influences to some extent the surface electronic structure. This may cause the shift of the surface plasmon resonance frequency and lead to the change of the local electric field at the metal surface.^{46e,81} Quantum mechanical schemes, describing the SERS enhancement based on the surface plasmon polariton model involving the interaction of the surface with the light, were suggested by several groups.⁸² As pointed out by Otto^{13a} and Pettinger,^{82a} the total process is a sequence consisting of the creation of the surface plasmon excitation, its inelastic scattering, and finally its annihilation by the radiating photons. More recently, a quantum chemical scheme has been performed by Corni et al. to calculate the surface enhancement factor and to analyze the shape and size effect of nanoparticles adsorbed by molecules.^{82e–g} Hopefully, this study can be further extended to the transition metals soon with the aid of more powerful computational methods.

5. Outlook and Summary

The recent advances of surface enhanced spectroscopy (including SERS, SEHRS, SEIRS, SESHG, and SESFG) provide good reason for renewing extensive interest in this field. One may be able to deepen our knowledge on issues related not only to surface-enhanced spectroscopy and surface processes but also nanoscience. Accordingly, we will briefly describe some possible developments in terms of the SERS substrate, with emphasize on the transition metal and technique as well as some relevant issues of surface science and nanoscience.

5.1. Ordered Nanostructured Surfaces. There is no doubt that along with the rapid development of the nanofabrication technique, well-controlled nanostructured surfaces will be prepared as a new class of highly SERS-active substrates. Two types of nanofabrication techniques, i.e., lithography and template synthesis, will probably play a dominant role for this purpose. Electron, ion, or light beam lithography^{83,84} and SPM (STM and AFM) lithography⁸⁵ can make highly ordered periodic arrays with optimized particle size, shape, and interparticle spacing. However, these point-by-point approaches make the fabrication process very slow. It is also quite difficult to fabricate nanostructures with a high aspect ratio. Nanostructured surfaces with a large area can be prepared more easily and quickly by the template synthesis technique,^{48,86} especially when combined with the self-assembly method,^{44,45} and sphere lithography.⁴⁶ Various materials can be filled controllably into a designed template of two-dimensional ordered nanopores (holes or channels). The template is then removed, leaving behind the spheroid, rod, or wire array with the desired aspect ratio. Because the template is generally formed by self-assembly, it is hard to control the interparticle spacing. It is therefore highly desirable to develop some methods to overcome this problem. Progress in fabricating these two-dimensional nanostructured surfaces will provide great opportunity for not only optimizing the SERS activity of existing materials but also searching for a new class of SERS active materials, such as bimetals, alloys, and sandwiched materials. With its extremely high sensitivity, SERS will further improve and expand its applicability, e.g., in the optical sensor and probably data storage.

5.2. Well-Defined Single-Crystal Surfaces. The strategy of extending the SERS substrate from the rough and ill-defined surface to the atomically flat and well-defined surface is also crucially important to develop SERS into a powerful tool in surface science. It should be pointed out that several groups have claimed that unenhanced Raman scattering can be detected from smooth surfaces of noble and transition metals.^{22c,23–25,26b} However, most of the surfaces were prepared using a series of emery paper, diamond, or alumina paste until the surface took on a mirror finish. From the point of view of the atomic structure, these surfaces are still ill-defined and consist of many SERS-active sites, such as ad-clusters that are chemically active and easily form the surface complex with the adsorbate. Only a few studies were carefully carried out on truly atomic flat surfaces, such as pyridine adsorbed on Ag and Pt single-crystal surfaces.^{8,15b,24b,67h} Nevertheless, the intrinsically low Raman cross section severely limits normal Raman spectroscopy to be widely used in surface science. The SERS obtained from atomically flat single crystal surfaces, if possible, will be greatly helpful for studying the orientation of adsorbates unambiguously and for comparing surface selection rules of conventional Raman spectroscopy and SERS. Moreover, the well-defined single crystal surface is completely different from the typical SERS active sites, which are generally ill-defined, including a wide variety of adatoms, ad-clusters, and surface complexes. The

former can have well-known electronic levels of metal or surface states, which are essential parameters for revealing the chemical mechanism, if it exists. Therefore, detailed comparison with the signal from well-defined single-crystal surfaces and rough surfaces can lead to a better understanding of the SERS mechanism.

A SERS study using an ATR Raman cell with the Otto configuration on truly smooth single-crystal surfaces under electrochemical conditions has been carried out recently.⁸⁷ The enhancement factor, assisted by the surface plasma enhancement, for a single-crystal Cu surface is estimated to be around 1–2 orders. Another type of ATR Raman cell with the Kretschmann configuration has also been used to obtain SERS from the Ag-(111) surface, as well as from Pt and Ni surfaces, without applying a potential.⁸⁸ It should be noted that, at present, there are only few molecules with large Raman cross section that can be used in this difficult investigation. As mentioned above, the surface plasmon enhancement is rather weak for transition metals. This technique seems not to be suitable to study single-crystal surface of the transition metal. Overall, the major challenge is to improve the detection sensitivity of Raman instrumentation and method to extend the study to a variety of molecules.

5.3. Tip-Enhanced Raman Spectroscopy. In addition to the ATR SERS, there is a promising and important approach to study smooth metal surfaces, which is named tip-enhanced surface Raman spectroscopy.⁸⁹ It combines Raman spectroscopy at smooth metal surfaces with an STM tip used as an amplifier of the electromagnetic field. This approach is generally applicable to metal/vacuum, metal/gas phase, or metal/electrolyte interfaces. An electrochemically etched Ag or Au wire is used as the STM tip. If the tip is in the tunneling position (with the tip–surface distance around 1 nm), the total Raman intensity increases by a factor of 15. Many bands, which were previously obscured by noise, are now clearly discernible. The field enhancement by the tunneling tip is due to the excitation of localized surface plasmons, which is also effective to the substrate areas in close proximity to the tip apex. Thus, the illuminated tip in the tunneling mode can induce the SERS of adsorbate at the smooth surface of any materials including transition metals. However, it suffers a serious drawback in the detection sensitivity. This may be overcome, at least partially, if one could fabricate then employ the two-dimensional tip array, such as the Ag or Au nanorod array, to replace the single tip used presently. This new technique belongs to the family of scanning near-field microscopy (SNOM) and shows great promise because of its very high spatial resolution. Recently, there are some reports concerning SNOM-SERS.⁹⁰ However, the sensitivity of both techniques is still too low to be applied to the study of transition-metal systems. The situation also happens to surface-enhanced hyper Raman spectroscopy (SEHRS),⁹¹ although SEHRS can provide complementary data for SERS. Therefore, how to improve the detection sensitivity is the major challenge for these techniques.

5.4. Well-Defined Nanostructured Surfaces. It should be noted that the above two kinds of surfaces are obviously in contrast to each other in morphology, and they have some advantages and disadvantages. As SERS is a nanostructure-based phenomenon, the atomically flat single crystal surface is surely neither the typical surface for SERS study nor the best surface exhibiting high SERS activity. Furthermore, the well-ordered nanostructured surface cannot exclude the inhomogeneity of the surface structure. It may still consist of many ill-defined structures at the atomic level, inevitably mixing up many energy

levels (surface states). It will make the quantitative analysis of the chemical enhancement very difficult or nearly impossible. Hence, we believe that the only solution is to construct the atomic-scale well-defined nanostructured surface.⁶⁴ Such a nanostructured surface has every nanostructured domain, i.e., nanocrystal, precisely prepared to have a well-defined surface facet and well-controlled internanocrystal space, as illustrated in Figure 13. It can further optimize the SERS activity, which will probably be the ultimate objective for the SERS substrate.

More importantly, this idealized surface structure may have far-reaching consequences with respect to other fields. It will probably bridge the gap between single crystal surfaces of fundamental interest and highly rough surfaces of practical importance and then eventually link surface science and nanoscale science. It has been known for a long time that highly rough surfaces are remarkably different from atomically flat (even stepped) single-crystal surfaces in chemical and physical properties. One classical example is that the former in general has substantially higher surface reactivity, e.g., for many transition metal based systems. Unfortunately, it is impossible so far to use in situ STM to study and clearly reveal the nature of the highly rough surface at the atomic level. Because the surface structure is distributed so heterogeneously, the theoretical modes are difficult to be developed based on the experimental data obtained from the ill-defined surfaces. Relying on the development of nanofabrication technique, we believe that this proposed approach would be realized eventually. This strategy will also provide a perfect model surface for the theoreticians to obtain a deeper insight into the surface chemical reaction mechanism. Furthermore, one may shed new light on the longstanding problem of whether there are any relations of SERS hot spots (active sites) and chemical active sites. This approach is essential for using SERS to study surface chemical reaction and processes unambiguously.

5.5. Probing the Optical Properties and Electronic Levels of Nanostructures and Surface Species. As some optical and electric properties change with size and shape of the metal nanoparticles, it makes the theoretical SERS study more difficult. However, once we have accumulated enough experimental data and formulated a relevant theory, SERS could be in turn to used to diagnose the special optical properties of various nanoparticles. For example, one can take the probe molecule strategy to correlate to the SERS spectral feature based on the EM theory. On the other hand, SERS may also be applied to probe the energetic levels of the adsorbate or the surface complex acted as the SERS active site based on the CT mechanism. By analyzing the shift in band frequency and the SERS intensity of the probe molecules, one can use the tunable laser to tune the incident photon energy to match the specific CT resonance. Considering the extreme difficulty of investigating in situ surface reaction states, SERS may provide a new way to detect the intermediate energy levels of surface species or the complex during the chemical reaction and adsorption processes. On the other hand, the ultrafast Raman spectroscopy⁹² and other spectroscopies with time resolutions ranging from picoseconds to femtoseconds⁹³ as well as the relevant theories⁹⁴ would be very powerful if they can be applied successfully in the SERS mechanism study. The ultrahigh time-resolution investigation on the SERS active systems can be very helpful for the detailed analyzing of the photon-driven charge-transfer process with every single step and path.

5.6. Summary. Through more than two decades of research effort by many groups including ours to challenge the key issue of whether transition metals are SERS active or not, it has now

been shown convincingly that SERS can be generated on transition metal substrates. The latest advances relied mainly on developing various fabricating procedures of nanostructured surfaces and optimizing the performance of the confocal Raman microscope. On the basis of the previous works on the noble metals, five methods to obtain transition metal substrates with SERS activity have been developed in our laboratory, i.e., potential-controlled ORC, current-controlled ORC, chemical etching, electrodeposition, and template synthesis. The last approach is aimed at replacing randomly roughened surfaces with ordered nanorod arrays having a narrow size-distribution. The calculated surface enhancement factors of seven roughened transition metals (Fe, Co, Ni, Ru, Rh, Pd, and Pt) ranged from 1 order to 4 orders of magnitude, depending on the metal and surface pretreatment. Successful applications in electrochemical adsorption, electrocatalysis, and corrosion of transition-metal-based systems demonstrate that SERS can be widely used to investigate diverse substrates that were commonly considered to be non-SERS active. On the basis of the previous works on EM and CT mechanisms, a preliminary theoretical approach is presented to explain SERS observed from transition metals. Although the interband electronic transition depresses the quality and changes the feature of the surface plasmon resonance, the lightning-rod effect seems to play the more important role to the EM enhancement for transition metals in comparison with noble metals. We estimated the enhancement factor from the pyridine adsorbed at the Co surfaces as one example. The surface averaging EM enhancement factor is about 2 orders and the CT enhancement factor is around 1 order. The progress on the SERS of transition metals and especially the significant development of single molecule SERS lead us to believe in a renaissance in SERS studies. We are optimistic that, along with developments in nanoscience, spectroscopy, and laser technology, many opportunities will emerge in the field of SERS to enhance our understanding of the surface-enhanced optical spectroscopy and to develop the technique into a versatile and powerful tool in surface science, nanoscience, materials science, analytical chemistry, electrochemistry, and catalysis.

Acknowledgment. This work was supported by the Natural Science Foundation of China and the Ministry of Education of China under the Contracts 29833060, 29903009, 20003008, 20021002, and 99177. We are very grateful to C. A. Melendres for providing much help in editing the English. Whenever the work from the authors' group is mentioned in the article, it is the contribution of the self-motivated and hard working students and all other group members.

References and Notes

- (1) (a) Fleischmann, M.; Hendra, P. J.; McQuillan, A. J. *Chem. Phys. Lett.* **1974**, *26*, 163. (b) Fleischmann, M.; Hendra, P. J.; McQuillan, A. J. *J. Chem. Soc., Chem. Commun.* **1973**, 80. (c) Fleischmann, M.; Hill, I. R. In *Comprehensive Treatise of Electrochemistry*; White, R. E., Bockris, J. O'M., Conway, B. E., Yeager, E., Eds.; Plenum Press: New York, 1984; Vol. 8, p 373.
- (2) (a) Jeanmaire, D. J.; Van Duyne, R. P. *J. Electroanal. Chem.* **1977**, *84*, 1. (b) Van Duyne, R. P. In *Chemical and Biochemical Applications of Lasers*; Moore, C. B., Eds.; Academic Press: New York, 1979; Vol. 4, p 101.
- (3) Albrecht, M. G.; Creighton, J. A. *J. Am. Chem. Soc.* **1977**, *99*, 5215.
- (4) (a) Chang, R. K.; Furtak, T. E. *Surface Enhanced Raman Scattering*; Plenum Press: New York, 1982. (b) Chang, R. K. *Ber. Bunsen-Ges. Phys. Chem.* **1987**, *91*, 296.
- (5) (a) Cotton, M. T. *Adv. Spectrosc.* **1988**, *16*, 91. (b) Garrell, R. L. *Anal. Chem.* **1989**, *61*, 401A. (c) Birke, R. L.; Lu, T.; Lombardi, J. R. In *Techniques for Characterization of Electrodes and Electrochemical Processes*; Varma, R., Selman, J. R., Eds.; John Wiley & Sons: New York, 1991; p 211. (d) Pemberton, J. E. In *In Situ Studies of Electrochemical Interfaces: A Prospectus*; Abruna, H. D., Ed.; VCH Verlag Chemie: Berlin,

- 1991; p 328. (e) Pettinger, B. In *Adsorption at Electrode Surface*; Lipkowsky, J., Ross, P. N., Eds.; VCH: New York, 1992; p 285. (f) Kneipp, K.; Kneipp, H.; Itzkan, I.; Dasari, R.; Feld, M. S. *Chem. Rev.* **1999**, *99*, 2957.
- (6) Schrotter, W. H.; Klockner, H. W. In *Raman Spectroscopy of Gases and Liquids*; Weber, A., Ed.; Springer-Verlag: Berlin, 1979; Vol. 11, p 123.
- (7) (a) Creighton, J. A.; Blatchford, C. G.; Albrecht, M. G. *J. Chem. Soc., Faraday II* **1979**, *75*, 790. (b) Pettinger, B.; Wenning, U. *Chem. Phys. Lett.* **1978**, *56*, 263.
- (8) Campion, A. In *Vibrational Spectroscopy of Molecules on Surface*; Yates, J. T., Madey, T. E., Eds.; Plenum: New York, 1987; Chapter 5, p 345.
- (9) (a) Moskovits, M. *Chem. Phys. Lett.* **1983**, *98*, 498. (b) Murray, C. A. In *Surface Enhanced Raman Scattering*; Chang, R. K., Dorain, P., Eds.; Plenum: New York, 1982; p 203.
- (10) (a) Dorain, P. B.; Von Raben, K. V.; Chang, R. K., Laube, B. L. *Chem. Phys. Lett.* **1981**, *84*, 405. (b) Krasser, W.; Renouprez, A. J. *Solid State Commun.* **1982**, *41*, 231.
- (11) (a) Kovacs, G. J.; Loufty, R. O.; Vincett, P. S.; Jennings, C.; Aroca, R. *Langmuir* **1986**, *2*, 689. (b) DiLella, D. P.; Zhou, P. *Chem. Phys. Lett.* **1990**, *166*, 240. (c) Lund, R. A.; Smardzewski, R. R.; Tevault, D. E. *J. Chem. Phys.* **1984**, *88*, 1731. (d) Gao, Y.; Lopez-Rios, T. *Surf. Sci.* **1988**, *198*, 509. (e) Loo, B. H. *J. Chem. Phys.* **1981**, *75*, 5955. (f) Brolo, A. G.; Odziemkowski, M.; Irish, D. E. *J. Raman Spectrosc.* **1998**, *29*, 713.
- (12) (a) Moskovits, M. *Rev. Mod. Phys.* **1985**, *57*, 783. (b) Moskovits, M. *J. Chem. Phys.* **1982**, *77*, 4408. (c) Moskovits, M.; Tay, L. L.; Yang, J.; Haslett, T. *Top. Appl. Phys.* **2002**, *82*, 215.
- (13) (a) Otto, A. In *Light Scattering in Solid*; Cardona, M., Guntherodt, G., Eds.; Springer-Verlag: Berlin, 1984; Vol. IV, p 289. (b) Otto, A.; Mrozek, I.; Grabhorn, H.; Akemann, W. *J. Phys. Condens. Matter* **1992**, *4*, 1143. (c) Otto, A. *Phys. Stat. Sol. A* **2001**, *188*, 1455.
- (14) (a) Kerker, M. *Acc. Chem. Res.* **1984**, *17*, 271. (b) Metiu, H.; Das, P. *Annu. Rev. Phys. Chem.* **1984**, *35*, 507. (c) Schatz, G. C. *Acc. Chem. Res.* **1984**, *17*, 370. (d) Creighton, J. A. In *Spectroscopy of Surface*; Clark, R. J. H., Hester, R. E., Eds.; John Wiley & Sons: New York, 1988; p 37. (e) Kerker, M.; Wang, S.; Chew, H. *Appl. Opt.* **1980**, *19*, 4159.
- (15) (a) Persson, B. N. J. *Chem. Phys. Lett.* **1981**, *82*, 561. (b) Campion, A.; Kambhampati, P. *Chem. Soc. Rev.* **1998**, *27*, 241. (c) Jiang, X.; Campion, A. *Chem. Phys. Lett.* **1987**, *140*, 95. (d) Arenas, J. F.; Woolley, M. S.; Lopez Tocon, I.; Otero, J. C.; Marcos, J. I. *J. Chem. Phys.* **2000**, *112*, 7669. (e) Arenas, J. F.; Tocon, I. L.; Otero, J. C.; Marcos, J. I. *J. Phys. Chem.* **1996**, *100*, 9254. (f) Adrian, F. J. *J. Chem. Phys.* **1982**, *77*, 5302. (g) Ueba, H. *Surf. Sci.* **1983**, *131*, 347. (h) Lombardi, J. R.; Birke, R. L.; Lu, T. H.; Xu, J. *J. Chem. Phys.* **1986**, *84*, 4174.
- (16) (a) Van Duyne, R. P.; Haushalter, J. P. *J. Phys. Chem.* **1983**, *87*, 7, 2999. (b) Cotton, T. M.; Van Duyne, R. P.; Rubim, J. C.; Kannen, G.; Schumacher, D.; Dunnwald, J.; Otto, A. *Appl. Surf. Sci.* **1989**, *37*, 233. (c) Feng, Q.; Cotton, T. M. *J. Phys. Chem.* **1986**, *90*, 983. (d) Oblonsky, L. J.; Devine, T. M.; Ager, J. W.; Perry, S. S.; Mao, X. L.; Russo, R. E. *J. Electrochem. Soc.* **1994**, *141*, 3312.
- (17) (a) Fleischmann, M.; Tian, Z. Q. *J. Electroanal. Chem.* **1987**, *217*, 385. (b) Fleischmann, M.; Tian, Z. Q.; Li, L. J. *J. Electroanal. Chem.* **1987**, *217*, 397. (c) Mengoli, G.; Musiani, M. M.; Fleischmann, M.; Mao, B. W.; Tian, Z. Q. *Electrochem. Acta* **1987**, *32*, 1239. (d) Aramaki, K.; Ohi, M.; Uehara, J. *J. Electrochem. Soc.* **1992**, *139*, 1525.
- (18) (a) Leung, L. W. H.; Weaver, M. J. *J. Electroanal. Chem.* **1987**, *217*, 367. (b) Leung, L. W. H.; Weaver, M. J. *J. Am. Chem. Soc.* **1987**, *109*, 5113. (c) Leung, L. W. H.; Weaver, M. J. *Langmuir* **1988**, *4*, 1076. (d) Zhang, Y.; Gao, X.; Weaver, M. J. *J. Phys. Chem.* **1993**, *97*, 8656.
- (19) (a) Zou, S.; Weaver, M. J. *Anal. Chem.* **1998**, *70*, 2387. (b) Zou, S. Z.; Williams, C. T.; Chen, E. K. Y.; Weaver, M. J. *J. Am. Chem. Soc.* **1998**, *120*, 3811. (c) Weaver, M. J.; Zou, S.; Chan, H. Y. H. *Anal. Chem.* **2000**, *72*, 38A. (d) Mrozek, M. F.; Luo, H.; Weaver, M. J. *Langmuir* **2000**, *16*, 8463. (e) Mrozek, M. F.; Xie, Y.; Weaver, M. J. *Anal. Chem.* **2001**, *73*, 5953.
- (20) (a) Gosztola, D.; Weaver, M. J. *J. Electroanal. Chem.* **1989**, *271*, 141. (b) Gui, J.; Devine, T. M. *J. Electrochem. Soc.* **1991**, *138*, 1376. (c) Melendres, C. A.; Pankuch, M.; Li, Y. S.; Knight, R. L. *Electrochem. Acta* **1992**, *37*, 2747. (d) Zhong, C. J.; Tian, Z. Q.; Tian, Z. W. *Sci. China B* **1990**, *1233*. (e) Xue, G.; Lu, Y.; Shi, G. *Polymer* **1994**, *35*, 2488. (f) Zou, S. Z.; Weaver, M. J. *Chem. Phys. Lett.* **1999**, *312*, 101. (g) Constantino, C. J. L.; Lemma, T.; Antunes, P. A.; Aroca, R. *Anal. Chem.* **2001**, *73*, 3674. (h) Aroca, R. F.; Constantino, C. J. L. *Langmuir* **2000**, *16*, 5425.
- (21) (a) Melendres, C. A.; Camillone, N.; Tipton, T. *Electrochim. Acta* **1989**, *34*, 281. (b) Melendres, C. A. In *Spectroscopic and Diffraction Techniques in Interfacial Electrochemistry*; Gutierrez, C., Melendres, C. A., Eds.; Kluwer Academic: Dordrecht, 1990; p 181.
- (22) (a) Cooney, R. P.; Fleischmann, M.; Hendra, P. J. *J. Chem. Soc. Chem. Commun.* **1977**, 235. (b) Cooney, R. P.; Hendra, P. J.; Fleischmann, M. *J. Raman Spectrosc.* **1977**, *6*, 264. (c) Fleischmann, M.; Sockalingum, D.; Musiani, M. M. *Spectrochim. Acta* **1990**, *46A*, 285.
- (23) (a) Pettinger, B.; Tiedemann, U. *J. Electroanal. Chem.* **1987**, *228*, 219. (b) Pettinger, B.; Friedrich, A.; Tiedemann, U. *J. Electroanal. Chem.* **1990**, *280*, 49.
- (24) (a) Bryant, M. A.; Loa, S. L.; Pemberton, J. E. *Langmuir* **1992**, *8*, 753. (b) Taylor, C. E.; Pemberton, J. E.; Goodman, G. G.; Schoenfish, M. H. *Appl. Spectrosc.* **1999**, *53*, 1212.
- (25) Maeda, T.; Sasaki, Y.; Horie, C.; Osawa, M. *J. Electron Spectrosc. Relat. Phenom.* **1993**, *64/65*, 381.
- (26) (a) Bilmes, S. A.; Rubim, J. C.; Otto, A.; Arvia, A. J. *Chem. Phys. Lett.* **1989**, *159*, 89. (b) Bilmes, S. A. *Chem. Phys. Lett.* **1990**, *171*, 141. (c) Shannon, C.; Campion, A. J. *Phys. Chem.* **1988**, *92*, 1385. (d) Guo, L.; Huang, Q. J.; Li, X. Y.; Yang, S. H. *Phys. Chem. Chem. Phys.* **2001**, *3*, 1661.
- (27) (a) Yamada, H.; Yamamoto, Y. *Chem. Phys. Lett.* **1981**, *77*, 520. (b) Yamada, H.; Yamamoto, Y. *Surf. Sci.* **1983**, *134*, 71.
- (28) (a) Cline, M. P.; Barber, P. W.; Chang, R. K. *J. Opt. Soc. Am.* **1986**, *B3*, 15. (b) Messinger, B. J.; Ulrich Von Raben, K.; Chang, R. K.; Barber, P. W. *Phys. Rev. B* **1981**, *24*, 649.
- (29) (a) Chen, C. Y.; de Castro, A. R. B.; Shen, Y. R. *Phys. Rev. Lett.* **1981**, *46*, 145. (b) Wokaun, A.; Bergman, J. G.; Heritage, J. P.; Glass, A. M.; Liao, P. F.; Olson, D. H. *Phys. Rev. B* **1981**, *24*, 849.
- (30) (a) Hatta, A.; Ohshima, T.; Suetaka, W. *Appl. Phys. A* **1982**, *A21*, 71. (b) Osawa, M. *Bull. Chem. Soc. Jpn.* **1997**, *70*, 2861. (c) Zhang, Z. J.; Imae, T. *J. Colloid Interface Sci.* **2001**, *233*, 99. (d) Osawa, M. *Top. Appl. Phys.* **2001**, *81*, 163.
- (31) (a) Lu, G. Q.; Sun, S. G.; Cai, L. R.; Chen, S. P.; Tian, Z. W.; Shiu, K.-K. *Langmuir* **2000**, *16*, 778. (b) Zheng, M. S.; Sun, S. G.; Chen, S. P. *J. Appl. Electrochem.* **2001**, *31*, 749.
- (32) Glass, A. M.; Liao, P. F.; Bergman, J. G.; Olson, D. H. *Opt. Lett.* **1980**, *5*, 368.
- (33) Baldelli, S.; Eppler, A. S.; Anderson, E.; Shen, Y. R.; Somorjai, G. A. *J. Chem. Phys.* **2000**, *113*, 5432.
- (34) (a) Nie, S.; Emory, S. R. *Science* **1997**, *275*, 1102. (b) Kneipp, K.; Harrison, G. R.; Emory, S. R.; Nie, S. *Chimia* **1999**, *53*, 35. (c) Corset, J.; Aubard, J. Surface Enhanced Raman Scattering: New Trends and Applications (Special Issue). *J. Raman Spectrosc.* **1999**, 29(8). (d) Tian, Z. Q.; Ren, B. *Progress in Surface Raman Spectroscopy*; Xiamen University Press: Xiamen, China, 2000. (e) Shalaev, V. M., Ed.; Optical Properties of Nanostructured Random Media. In *Topics in Applied Physics* **82**, Springer-Verlag: Berlin, 2002.
- (35) (a) Chase, B. *Appl. Spectrosc.* **1994**, *48*(7), 14A. (b) Turrell, G.; Corset, J. *Raman Microscopy*; Academic Press: San Diego, 1996. (c) Tian, Z. Q.; Ren, B. *Encyclopedia of Analytical Chemistry*; John Wiley & Sons: Chichester, 2000; p 9162.
- (36) (a) Tian, Z. Q.; Ren, B.; Mao, B. W. *J. Phys. Chem. B* **1997**, *101*, 1338. (b) Tian, Z. Q.; Gao, J. S.; Li, X. Q.; Ren, B.; Huang, Q. J.; Cai, W. B.; Liu, F. M.; Mao, B. W. *J. Raman Spectrosc.* **1998**, *29*, 703. (c) Cai, W. B.; Ren, B.; Li, X. Q.; She, C. X.; Liu, F. M.; Cai, X. W.; Tian, Z. Q. *Surf. Sci.* **1998**, *406*, 9. (d) Huang, Q. J.; Li, X. Q.; Yao, J. L.; Ren, B.; Cai, W. B.; Gao, J. S.; Mao, B. W.; Tian, Z. Q. *Surf. Sci.* **1999**, *427/428*, 162.
- (37) (a) Ren, B.; Huang, Q. J.; Cai, W. B.; Mao, B. W.; Liu, F. M.; Tian, Z. Q. *J. Electroanal. Chem.* **1996**, *415*, 175. (b) Gao, J. S.; Tian, Z. Q. *Spectrochim. Acta* **1997**, *A 53*, 1595. (c) Huang, Q. J.; Yao, J. L.; Gu, R. A.; Tian, Z. Q. *Chem. Phys. Lett.* **1997**, *271*, 101. (d) Cao, P. G.; Yao, J. L.; Ren, B.; Mao, B. W.; Gu, R. A.; Tian, Z. Q. *Chem. Phys. Lett.* **2000**, *316*, 1. (e) Wu, D. Y.; Xie, Y.; Ren, B.; Yan, J. W.; Mao, B. W.; Tian, Z. Q. *Phys. Chem. Commun.* **2001**, *18*, 1.
- (38) (a) Kneipp, K.; Wang, Y.; Kneipp, H.; Perelman, L. T.; Itzkan, I.; Dasari, R. R.; Feld, M. S. *Phys. Rev. Lett.* **1997**, *78*, 1667. (b) Kneipp, K.; Kneipp, H.; Itzkan, I.; Dasari, R. R.; Feld, M. S. *Chem. Rev.* **1999**, *99*, 2957. (c) Kneipp, K.; Kneipp, H.; Itzkan, I.; Dasari, R. R.; Feld, M. S.; Dresselhaus, M. S. *Top. Appl. Phys.* **2002**, *82*, 227.
- (39) (a) Emory, S. R.; Nie, S. *J. Am. Chem. Soc.* **1998**, *120*, 8009. (b) Emory, S. R.; Nie, S. *J. Phys. Chem. B* **1998**, *102*, 493. (c) Krug, J. T.; Wang, G. D.; Emory, S. R.; Nie, S. *J. Am. Chem. Soc.* **1999**, *121*, 9208. (d) Doering, W. E.; Nie, S. *J. Phys. Chem. B* **2002**, *106*, 311.
- (40) (a) Xu, H. X.; Bjerneld, E. J.; Kall, M.; Borjesson, L. *Phys. Rev. Lett.* **1999**, *83*, 4357. (b) Xu, H. X.; Aizpurua, J.; Kall, M.; Apell, P. *Phys. Rev. E* **2000**, *62*, 4318. (c) Michaels, M.; Nirmal, M.; Brus, L. E. *J. Am. Chem. Soc.* **1999**, *121*, 9932. (d) Michaels, M.; Jiang, J.; Brus, L. E. *J. Phys. Chem. B* **2000**, *104*, 11965. (e) Eggeling, C.; Schaffer, J.; Seidel, C. A. M.; Korte, J.; Brehm, G.; Schneider, S.; Schrof, W. *J. Phys. Chem. A* **2001**, *105*, 3673.
- (41) (a) Furtak, T. E.; Trott, G.; Loo, B. H. *Surf. Sci.* **1980**, *101*, 374. (b) Pockrand, I.; Otto, A. *Solid State Commun.* **1981**, *38*, 1159. (c) Welzel, H. A.; Gerischer, H.; Pettinger, B. *Chem. Phys. Lett.* **1981**, *80*, 392. (d) Watanabe, T.; Yanagihara, N.; Honda, K.; Pettinger, B.; Moerl, L. *Chem. Phys. Lett.* **1983**, *96*, 649. (e) Macomber, S. H.; Furtak, T. E. *Chem. Phys. Lett.* **1982**, *90*, 59. (f) Sueoka, T.; Inukai, J.; Ito, M. *J. Electron Spectrosc. Related Phenom.* **1993**, *64/65*, 363.
- (42) (a) Tsai, D. P.; Kovacs, J.; Wang, Z.; Moskovits, M.; Shalaev, V. M.; Suh, J. S.; Botet, R. *Phys. Rev. Lett.* **1994**, *72*, 4149. (b) Zhang, P.; Haslett, T. L.; Douketis, C.; Moskovits, M. *Phys. Rev. B* **1998**, *57*, 15513.

- (c) Markel, V. A.; Shalaev, V. M.; Zhang, P.; Huynh, W.; Tay, L.; Haslett, T. L.; Moskovits, M. *Phys. Rev. B* **1999**, 59, 10903. (d) Haslett, T. L.; Tay, L.; Moskovits, M. *J. Chem. Phys.* **2000**, 113, 1641. (f) Shalaev, V. M. *Phys. Rep.* **1996**, 272, 61. (g) Sarychev, A.; Shalaev, V. M. *Phys. Rep.* **2000**, 335, 275.
- (43) (a) Liao, P. F.; Bergman, J. G.; Chemla, D. S.; Wokaun, A.; Melngailis, J.; Hawryluk, A. M.; Economou, N. P. *Chem. Phys. Lett.* **1981**, 82, 355. (b) Liao, P. F.; Stern, M. B. *Opt. Lett.* **1982**, 7, 483.
- (44) (a) Nicewarner-Pena, S. R.; Freeman, R. G.; Reiss, B. D.; He, L.; Pena, D. J.; Walton, I. D.; Cromer, R.; Keating, C. D.; Natan, M. J. *Science* **2001**, 294, 137. (b) Musick, M. D.; Keating, C. D.; Lyon, L. A.; Botsko, S. L.; Pena, D. J.; Holliday, W. D.; McEvoy, T. M.; Richardson, J. N.; Natan, M. J. *Chem. Mater.* **2000**, 12, 2869. (c) Martin, B. R.; Dermody, D. J.; Reiss, B. D.; Fang, M. M.; Lyon, L. A.; Natan, M. J.; Mallouk, T. E. *Adv. Mater.* **1999**, 11, 1021. (d) Keating, C. D.; Kovaleski, K. K.; Natan, M. J. *J. Phys. Chem. B* **1998**, 102, 9414. (e) Musick, M. D.; Keating, C. D.; Keefe, M. H.; Natan, M. J. *Chem. Mater.* **1997**, 9, 1499.
- (45) (a) Vo-Dinh, T. *Trac-Trend Anal. Chem.* **1998**, 17, 557. (b) Zhu, T.; Yu, H. Z.; Wang, J.; Wang, Y. Q.; Cai, S. M.; Liu, Z. F. *Chem. Phys. Lett.* **1997**, 265, 334. (c) He, H. X.; Zhang, H.; Li, Q. G.; Zhu, T.; Li, S. Y.; Liu, Z. F. *Langmuir* **2000**, 16, 3846. (d) Huang, X. H.; Huang, H. Z.; Wu, N. Z.; Hu, R. S.; Zhu, T.; Liu, Z. F. *Surf. Sci.* **2000**, 459, 183.
- (46) (a) Hulstee, J. C.; Treichel, D. A.; Smith, M. T.; Duval, M. L.; Jensen, T. R.; Van Duyne, R. P. *J. Phys. Chem. B* **1999**, 103, 3854. (b) Jensen, T. R.; Malinsky, M. D.; Haynes, C. L.; Van Duyne, R. P. *J. Phys. Chem. B* **2000**, 104, 10549. (c) Malinsky, M. D.; Kelly, K. L.; Schatz, G. C.; Van Duyne, R. P. *J. Phys. Chem. B* **2001**, 105, 2343. (d) Haynes, C. L.; Van Duyne, R. P. *J. Phys. Chem. B* **2001**, 105, 5599. (e) Malinsky, M. D.; Kelly, K. L.; Schatz, G. C.; Van Duyne, R. P. *J. Am. Chem. Soc.* **2001**, 123, 1471. (f) Dick, L. A.; McFarland, A. D.; Haynes, C. L.; Van Duyne, R. P. *J. Phys. Chem. B* **2002**, 106, 853.
- (47) Park, S.; Yang, P.; Corredor, P.; Weaver, M. J. *J. Am. Chem. Soc.* **2002**, 124, 2428.
- (48) (a) Martin, C. R. *Science* **1994**, 266, 1961. (b) Masuda, H.; Fukuka, K. *Science* **1995**, 268, 1466. (c) Routkevitch, D.; Haslett, T. L.; Ryan, L.; Bigioni, T.; Douketis, C.; Moskovits, M. *J. Chem. Phys.* **1996**, 210, 343. (d) Joo, Y.; Suh, J. S. *Bull. Korean Chem. Soc.* **1995**, 16, 808. (e) Suh, J. S.; Lee, J. S. *Chem. Phys. Lett.* **1997**, 281, 384. (f) Yao, J. L.; Pan, G. P.; Xue, K. H.; Wu, D. Y.; Ren, B.; Sun, D. M.; Tang, J.; Xu, X.; Tian, Z. Q. *Pure Appl. Chem.* **2000**, 72, 221. (g) Yao, J. L.; Tang, J.; Wu, D. Y.; Sun, D. M.; Xue, K. H.; Ren, B.; Mao, B. W.; Tian, Z. Q. *Surf. Sci.* **2002**, 514, 108.
- (49) (a) Behringer, J.; Brandmuller, J. Z. *Elektrochem.* **1956**, 60, 643. (b) Galabar, B. S.; Dudev, *Vibrational Spectra and Structure: Vibrational Intensities*; Durig, J. R., Ed.; Elsevier: Amsterdam, 1996.
- (50) (a) Chialvo, A. C.; Triaca, W. E.; Arvia, A. J. *J. Electroanal. Chem.* **1983**, 146, 93. (b) Visintin, A.; Triaca, W. E.; Arvia, A. J. *J. Electroanal. Chem.* **1987**, 221, 239.
- (51) Ren, B.; Lin, X. F.; Tian, Z. Q. In *Progress in Surface Raman Spectroscopy*; Tian, Z. Q., Ren, B., Eds.; Xiamen University Press: Xiamen, China, 2000; p 91.
- (52) (a) Kordesch, M. E.; Stenzel, W.; Conard, H. *Surf. Sci.* **1987**, 186, 601. (b) Carron, K. T.; Xue, G.; Lewis, M. L. *Langmuir* **1991**, 7, 2. (c) Xue, G.; Dong, J. *Anal. Chem.* **1991**, 63, 2393.
- (53) (a) Ren, B.; Li, X. Q.; She, C. X.; Wu, D. Y.; Tian, Z. Q. *Electrochim. Acta* **2000**, 46, 193. (b) Ren, B.; Jiang, Y. X.; Tian, Z. Q. In preparation.
- (54) Wiberg, K. B.; Walters, V. A.; Wong, K. N.; Colson, S. D. *J. Phys. Chem.* **1984**, 88, 6067.
- (55) (a) Abruña, H. D., Ed.; *Electrochemical Interfaces-Modern Techniques for in situ Characterization*; VCH: New York, 1991. (b) Christensen, P. A.; Hammett, A., Eds.; *Techniques and mechanisms in electrochemistry*; Chapman & Hall: London, 1993; Chapter 2. (c) Wieckowski, A., Ed.; *Interfacial Electrochemistry*; Marcel Dekker: New York, 1999.
- (56) Bockris, J. O'M.; Reddy, A. K. N. *Modern electrochemistry*; Kluwer/Plenum: New York, 1998.
- (57) Nakamoto, K. *Infrared and Raman Spectra of Inorganic and Coordination Compounds*, 3rd ed.; Wiley: New York, 1978.
- (58) (a) Lipkowsky, J.; Ross, P. N., Eds.; *Electrocatalysis*; Wiley-VCH: New York, 1998. (b) Parsons, R.; Van der Noot, T. *J. Electroanal. Chem.* **1988**, 257, 9.
- (59) She, C. X.; Wang, X. C.; Ren, B.; Lin, H. S.; Tian, Z. Q. *Fudan Univ. Acta* **2002**, 41, 280.
- (60) (a) Watanabe, M.; Motoo, S. *J. Electroanal. Chem.* **1975**, 60, 267. (b) Jarvi, T. D.; Stuve, E. M. In *Electrocatalysis*; Lipkowsky, J., Ross, P. N., Eds.; Wiley-VCH: New York, 1998.
- (61) Melendres, C. A.; Camillone, N.; Tipton, T. *Electrochim. Acta* **1989**, 34, 281.
- (62) Kester, J. J.; Furtak, T. E.; Bevolio, A. J. *J. Electrochem. Soc.* **1982**, 129, 1716.
- (63) (a) Yao, J. L.; Ren, B.; Huang, Z. F.; Cao, P. G.; Gu, R. A.; Tian, Z. Q. *Electrochim. Acta* **2002**, in press. (b) Cao, P. G.; Yao, J. L.; Zheng, J. W.; Gu, R. A.; Tian, Z. Q. *Langmuir* **2002**, 18, 100. (c) Cao, P. G.; Yao, J. L.; Ren, B.; Gu, R. A.; Tian, Z. Q. *J. Phys. Chem. B* **2002**, in press.
- (64) (a) Tian, Z. Q.; Ren, B.; Wu, D. Y.; Mao, B. W.; Xu, Y. F. *J. Xiamen University* **2001**, 40, 434. (b) Tian, Z. Q. *China Basic Sci.* **2001**, 3, 4.
- (65) (a) Gersten, J.; Nitzan, A. *J. Chem. Phys.* **1980**, 73, 3023. (b) Adrian, F. J. *Chem. Phys. Lett.* **1981**, 78, 45. (c) Metiu, H. *Prog. Surf. Sci.* **1984**, 17, 153. (d) Metiu, In *Surface-enhanced Raman Scattering*; Furtak, T. E., Chang, R. K., Eds.; Plenum: New York, 1981. (e) Schatz, G. C.; van Duyne, R. P. In *Handbook of Vibrational Spectroscopy*; Chalmers, J. M., Griffiths, P. R., Eds.; John Wiley & Sons: Chichester, 2002.
- (66) (a) Garcia-Vidal, F. J.; Pendry, J. B. *Phys. Rev. Lett.* **1996**, 77, 1163. (b) Kottmann, J. P.; Martin, O. J. F.; Smith, D. R.; Schultz, S. *Chem. Phys. Lett.* **2001**, 314, 1. (c) Kottmann, J. P.; Martin, O. J. F.; Smith, D. R.; Schultz, S. *Opt. Exp.* **2000**, 6, 213. (d) Kottmann, J. P.; Martin, O. J. F.; Smith, D. R.; Schultz, S. *Phys. Rev. B* **2001**, 64, 235402.
- (67) (a) Burstein, E.; Chen, Y. J.; Chen, C. Y.; Lundquist, S.; Tossatti, E. *Solid State Commun.* **1979**, 29, 567. (b) Gersten, J. I.; Birke, R. L.; Lombardi, J. R. *Phys. Rev. Lett.* **1979**, 43, 147. (c) Otto, A. *Surf. Sci.* **1980**, 92, 145. (d) Billman, J.; Otto, A. *Surf. Sci.* **1984**, 138, 1. (e) Otto, A.; Billmann, J.; Eickmans, J.; Erturk, U.; Pettenkofer, C. *Surf. Sci.* **1984**, 138, 319. (f) Creighton, J. A. *Surf. Sci.* **1986**, 173, 665. (g) Arenas, J. F.; Tocon, I. L.; Otero, J. C.; Marcos, J. I. *J. Phys. Chem.* **1996**, 100, 9254. (h) Kambhampati, P.; Child, C. M.; Foster, M. C.; Campion, A. *J. Chem. Phys.* **1998**, 108, 5013.
- (68) (a) Birke, R. L.; Lombardi, J. R. In *Spectroelectrochemistry-Theory and practice*; Gale, R. J., Ed.; Plenum: New York, 1988; p 263. (b) Allen, C. S.; Van Duyne, R. P. *Chem. Phys. Lett.* **1979**, 63, 455. (c) Moskovits, M.; DiLella, D. P.; Maynard, K. J. *Langmuir* **1988**, 4, 67. (d) Gao, X.; Davies, J. P.; Weaver, M. J. *J. Phys. Chem.* **1990**, 94, 6858.
- (69) (a) Weaver, J. H. *Phys. Rev. B* **1975**, 11, 1416. (b) Ordal, M. A.; Bell, R. J.; Alexander, R. W., Jr.; Long, L. L.; Querry, M. R. *Appl. Opt.* **1985**, 24, 4493.
- (70) (a) Jensen, T. R.; Schatz, G. C.; Van Duyne, R. P. *J. Phys. Chem.* **1999**, 103, 2394. (b) Schatz, G. C. *J. Mol. Struct. (THEOCHEM)* **2001**, 573, 73.
- (71) Sanchez-Gil, J. A.; Garacia-Ramos, J. V. *J. Chem. Phys.* **1998**, 108, 317.
- (72) (a) Draine, B. T.; Flatau, P. J. *J. Opt. Soc. Am. A* **1994**, 11, 1491. (b) Draine, B. T.; Flatau, P. J. *User's Guide to the discrete Dipole Approximation code DDSCAT*, version 5a10; <http://xxx.lanl.gov/abs/astro-ph/0008151v2>, 2000.
- (73) Lippitsch, M. E. *Phys. Rev. B* **1984**, 29, 3101.
- (74) (a) Wu, D. Y.; Cao, Z. J.; Ren, B.; Xu, X.; Tian, Z. Q. *Chinese J. Light Scatt.* **2002**, 13, 199. (b) Wu, D. Y.; Xie, Y.; Ren, B.; Xu, X.; Tian, Z. Q. *J. Phys. Chem. B* **2002**, 106, in press.
- (75) (a) Kudelski, A.; Bukowska, J. *Chem. Phys. Lett.* **1994**, 222, 555. (b) Kudelski, A.; Bukowska, J.; Janik-Czachor, M.; Grochala, W.; Szummer, A.; Dolata, M. *Vib. Spectrosc.* **1998**, 16, 21.
- (76) Rubim, J. C.; Corio, P.; Ribeiro, M. C. C.; Matz, M. *J. Phys. Chem.* **1995**, 99, 15765.
- (77) (a) Nenner, I.; Schulz, G. J. *J. Chem. Phys.* **1975**, 62, 1747. (b) Zylka, G.; Otto, A. *Surf. Sci.* **2001**, 475, 118. (c) Zhang, Q.; Gahl, C.; Wolf, M. *Surf. Sci.* **2002**, 496, 21.
- (78) (a) Creighton, J. A. In *Progress in Surface Raman Spectroscopy*; Tian, Z. Q., Ren, B., Eds.; Xiamen University Press: Xiamen, China, 2000; p 11. (b) Bauernschmitt, R.; Ahlrichs, R. *Chem. Phys. Lett.* **1996**, 256, 454.
- (79) (a) Clark, R. J. H.; Dines, T. *Angew. Chem., Int. Ed. Engl.* **1986**, 25, 131. (b) Albrecht, A. C. *J. Chem. Phys.* **1961**, 34, 1476.
- (80) (a) Chinsky, L.; Laigle, A.; Petcolas, W. L.; Turpin, P.-Y. *J. Chem. Phys.* **1982**, 76, 1. (b) Manneback, C. *Physica* **1951**, 17, 1001.
- (81) (a) Kim, X. W.; Villagran, E.; Even, U.; Thompson, J. C. *J. Chem. Phys.* **1991**, 94, 3974. (b) Persson, B. N. J. *Surf. Sci.* **1993**, 281, 153.
- (82) (a) Pettinger, B. *J. Chem. Phys.* **1986**, 85, 7442. (b) Arya, K.; Zeyher, R. *Phys. Rev. B* **1981**, 24, 1852. (c) Gies, P. *Phys. Rev. B* **1988**, 37, 10020. (d) Lee, T. K.; Birman, J. L. *Phys. Rev. B* **1980**, 22, 5961. (e) Corni, S.; Tomasi, J. *Chem. Phys. Lett.* **2001**, 342, 135. (f) Corni, S.; Tomasi, J. *J. Chem. Phys.* **2001**, 114, 3739. (g) Corni, S.; Tomasi, J. *J. Chem. Phys.* **2002**, 116, 1156.
- (83) (a) Notargiacomo, A.; Giovine, E.; Evangelisti, F.; Foglietti, V.; Leoni, R.; *Mater. Sci. Eng. C* **2002**, 19, 185. (b) Eppler, A. S.; Zhu, J.; Anderson, E. A.; Somorjai, G. A. *Top. Catal.* **2000**, 13, 33.
- (84) (a) Gunnarsson, L.; Petronis, S.; Kasemo, B.; Xu, H.; Bjerneld, J.; Kall, M. *Nanostruct. Mater.* **1999**, 12, 783. (b) Gunnarsson, L.; Bjerneld, E. J.; Xu, H.; Petronis, S.; Kasemo, B. *Appl. Phys. Lett.* **2001**, 78, 802.
- (85) (a) Kolb, D. M.; Ullmann, R.; Will, T. *Science* **1997**, 275, 1097. (b) Piner, R. D.; Zhu, J.; Xu, F.; Hong, S. H.; Mirkin, C. A. *Science* **1999**, 283, 661.
- (86) (a) Whitney, T. M.; Jiang, J. S.; Searson, P. C.; Chien, C. L. *Science* **1993**, 261, 1316. (b) Preston, C. K.; Moskovits, M. *J. Phys. Chem.* **1993**, 97, 8495. (c) Routkevitch, D.; Haslett, T. L.; Ryan, L.; Bigioni, T.; Douketis, C.; Moskovits, M. *J. Chem. Phys.* **1996**, 210, 343.

- (87) Bruckbauer, A.; Otto, A. *J. Raman. Spectrosc.* **1998**, 29, 665.
- (88) (a) Futamata, M. *Surf. Sci.* **1997**, 89, 386. (b) Futamata, M.; Bruckbauer, A. *Chem. Phys. Lett.* **2001**, 341, 425.
- (89) (a) Stockle, R.; Suh, Y. D.; Deckert, V.; Zenobi, R. *Chem. Phys. Lett.* **2000**, 318, 131. (b) Pettinger, B.; Picardi, G.; Schuster, R.; Ertl, G. *Electrochemistry* **2000**, 68, 942.
- (90) (a) Futamata, M.; Bruckbauer A. *Chem. Phys. Lett.* **2001**, 341, 425. (b) Futamata, M. *Chem. Phys. Lett.* **2001**, 333, 337. (c) Fokas, C.; Deckert, V. *Appl. Spectrosc.* **2002**, 56, 192.
- (91) (a) Golab, J. T.; Sprague, J. R.; Carron, K. T.; Schatz, G. C.; Van Duyne, R. P. *J. Chem. Phys.* **1988**, 88, 7942. (b) Kneipp, K.; Kneipp, H.; Itzkan, I.; Dasari, R. R.; Feld, M. S. *Chem. Phys.* **1999**, 247, 155. (c) Li, W. H.; Li, X. Y.; Yu, N. T. *Chem. Phys. Lett.* **1999**, 305, 303. (d) Li, W. H.; Li, X. Y.; Yu, N. T. *Chem. Phys. Lett.* **2000**, 327, 153.
- (92) (a) Pausch, R.; Heid, M.; Chen, T.; Kiefer, W.; Schwoerer, H. *J. Chem. Phys.* **1999**, 110, 9560. (b) Pausch, R.; Heid, M.; Chen, T.; Schwoerer, H.; Kiefer, W. *J. Raman Spectrosc.* **2000**, 31, 7.
- (93) (a) Asbury, J. B.; Hao, E.; Wang, Y. Q.; Ghosh, H. N.; Lian, T. Q. *J. Chem. Phys. B* **2001**, 105, 4545. (b) Ghosh, H. N.; Asbury, J. B.; Lian, T. Q. *J. Chem. Phys. B* **1998**, 102, 6482.
- (94) (a) Yang, T. S.; Chang, M. S.; Chang, R.; Hayashi, M.; Lin, S. H.; Vohringer, P.; Dietz, W.; Scherer, N. F. *J. Chem. Phys.* **1999**, 110, 12070. (b) Hayashi, M.; Yang, T. S.; Chang, C. H.; Liang, K. K.; Chang, R. L.; Lin, S. H. *Int. J. Quantum Chem.* **2000**, 80, 1043.